Chapter 1

Tropical Cyclone Structure and Dynamics

Jeffrey D. Kepert
Centre for Australian Weather and Climate Research,
Bureau of Meteorology, Melbourne Vic 3000, Australia
J.Kepert@bom.gov.au

Tropical cyclones are intense warm-cored cyclonic vortices that form over warm tropical oceans. Tropical cyclones can vary significantly from one to another, and from day to day, in intensity, size, boundary layer structure, spiral banding, eye structure and degree of symmetry. Significant progress has been made in understanding the factors that determine these differences and govern the storms' evolution. In particular, major advances have occurred in our understanding of the tropical cyclone boundary layer, of the dynamics and role of spiral bands, and of the interaction between the cyclone and its environment. This chapter reviews tropical cyclone structure and structure change, with an emphasis on these advances in knowledge since the last volume in this series.

1. Introduction

Tropical cyclones are intense atmospheric vortices that form over the warm tropical oceans. The inner part of the storm becomes nearly axisymmetric as the storm reaches maturity, and its strongest winds surround a relatively calm eye, whose diameter is typically in the range of 20 to 100 km. The pressure deficit in the eye can reach 10% of the ambient pressure, and hydrostatic calculations show that such a marked deficit requires that the cyclone's warm core extend through much of the troposphere (Haurwitz, 1935). The eye is partly or wholly surrounded by a ring of deep convective cloud that rises from just above the sea surface to the tropopause, sloping outwards as it rises, and which contains the strongest winds. In intense storms, this eyewall takes the appearance of a giant amphitheatre. The symmetric component of the cyclonic winds is nearly in gradient wind balance except in the surface frictional boundary layer and the outflow layer. The warm core aloft and gradient balance imply that the strength of the wind decreases with height above the boundary layer.

Superimposed on the dominant primary axisymmetric circulation are a weaker symmetric secondary circulation and various asymmetries. The secondary circulation consists of inflow concentrated in the boundary layer, upflow in the eyewall and spiral rainbands, and outflow in a thin layer beneath the tropopause. Surface friction and latent heat release are responsible for the secondary circulation, while interactions with surrounding weather systems also contribute at times. Air-sea exchange processes in the boundary layer weaken the storm due to momentum transfer to the sea, contribute to the secondary circulation, and provide energy through enthalpy fluxes from the sea (Ooyama, 1969). Angular momentum imported by the friction-induced component of the secondary circulation is largely or entirely destroyed by friction, but the diabatically forced component of the secondary circulation can provide a net import of angular momentum to spin up the storm. The latent heat release within the eyewall may also cause subsidence within the eye, creating the warm core and also the characteristic cloud-free circle near the middle of the central dense overcast on satellite images of

GLOBAL PERSPECTIVES ON TROPICAL CYCLONES - From Science to Mitigation

http://www.worldscibooks.com/environsci/7597.html

intense storms. The upper tropospheric outflow layer is markedly less symmetric than the rest of the storm, and may feature anticyclonic absolute vorticity and hence inertial instability. The tendency for stronger environmental winds and potential vorticity gradients in the upper troposphere contributes to these outflow asymmetries.

Asymmetries of the inner core can consist of transient propagating features due to instabilities of the basic flow, or of longer-lived quasi-stationary features resulting from interactions between the cyclone and its environment. Such asymmetries usually have a signal in the kinematic, thermodynamic and cloud fields. The most intense storms are usually more symmetric. Outside the core region, the storm grades smoothly into its environment. As the stabilising effect of the strong rotation in the inner core recedes, the strengths of the symmetric and asymmetric flow become comparable.

The lifecycle of tropical cyclones ranges from a day or two up to several weeks. In the early stages, the primary circulation is weak and is usually slow to build strength and symmetry. This chapter mostly applies to storms with maximum surface winds exceeding 15–20 $\mathrm{m\,s^{-1}}$, while the earlier phase is considered in Chapter 2. The aim here is to describe the structure of a mature storm in the context of its dynamics and thermodynamics. This chapter has a strong bias towards recent progress on understanding mature structure, whilst endeavouring to include sufficient of the earlier material to be reasonably self-contained. In particular, there is a deliberate focus on the important recent advances in understanding the boundary layer (section 5), on the dynamics and consequences of waves and instabilities (section 7), and on the response of the storm to its environmental (section 8). The fundamentally important secondary circulation and its role in the cyclones intensification is described in section 3, leading to theories of potential intensity in section 4. Parametric wind models are updated in section 6. Predecessors to the present chapter (Holland, 1987; Willoughby, 1995) are warmly recommended to those readers wanting more detail on other matters. Similarly, readers with a particular interest in air-sea interaction, the observational diagnosis of structure and structure change, or in forecast techniques, are referred to the appropriate chapters in this volume.

2. Equations and Balance Considerations

In the nearly axisymmetric cyclone core, storm-centred cylindrical coordinates are appropriate and the equations of motion may be written:

$$\frac{du}{dt} - \left(f + \frac{v}{r}\right) v = -\frac{1}{\rho}\frac{\partial p}{\partial r} + \frac{\partial \overline{u'w'}}{\partial z} \quad (1)$$

$$\frac{dv}{dt} + \left(f + \frac{v}{r}\right) u = -\frac{1}{r\rho}\frac{\partial p}{\partial \lambda} + \frac{\partial \overline{v'w'}}{\partial z} \quad (2)$$

$$\frac{dw}{dt} = -\frac{1}{\rho}\frac{\partial p}{\partial z} - g \quad (3)$$

$$\frac{\partial \rho}{\partial t} + \frac{1}{r}\frac{\partial \rho r u}{\partial r} + \frac{1}{r}\frac{\partial \rho v}{\partial \lambda} + \frac{\partial \rho w}{\partial z} = 0 \quad (4)$$

$$\frac{d\theta}{dt} = \dot{\theta} + \frac{\partial \overline{\theta'w'}}{\partial z} \quad (5)$$

$$\frac{dq}{\partial t} = E + \frac{\partial \overline{q'w'}}{\partial z} \quad (6)$$

$$\theta = T\left(\frac{p_0}{p}\right)^{R/c_p} \quad (7)$$

$$p = \rho R_d T_v \quad (8)$$

$$T_v = T[1 + q(1/\epsilon - 1)] \approx T(1 + 0.608q) \quad (9)$$

where the meanings of all symbols are given in Table 2. In these equations, some small terms have been omitted, including the horizontal components of the turbulent flux and the vertical components of the Coriolis acceleration. While their neglect is well justified in most of the atmosphere, it is less supported but conventional to do so in the tropical cyclone core.

These equations may be applied either in a coordinate system fixed to the earth's surface at the instantaneous cyclone location, or in one moving with the storm. In the latter case, the storm movement vector should strictly be constant, since otherwise extra terms are needed in the equations to account for the acceleration of the coordinate system.

In tropical cyclones, as elsewhere in the atmosphere, many of these equations contain two or three terms that are in approximate balance, with the remaining terms being substantially smaller. For instance, friction and radial accelerations are small except in the boundary and outflow layers. Equation (1) reduces (for storm-following coordinates) to the gradient wind equation,

$$\frac{v_{gr}^2}{r} + f v_{gr} = \frac{1}{\rho}\frac{\partial p}{\partial r}. \tag{10}$$

Similarly, (3) reduces to the hydrostatic equation,

$$\frac{\partial p}{\partial z} \approx -\rho g \tag{11}$$

although this approximation is less satisfactory in the eyewall, where larger vertical accelerations and small horizontal scales prevail. Combining (10) and (11) with (8) yields a gradient-wind form of the thermal wind equation,

$$\xi \frac{\partial v}{\partial \log p} \approx -R_d \frac{\partial T_v}{\partial r} \tag{12}$$

where the inertia parameter $\xi = 2v/r + f$ replaces f in the normal geostrophic form of the equation. From (12), a warm cored vortex will have cyclonic winds decreasing with height.

The vertical component of the absolute angular momentum

$$M_a = rv + f_0 r^2/2 \tag{13}$$

where f_0 is the Coriolis parameter at the cyclone centre, is useful for developing physical understanding, as the azimuthal momentum equation (2) may be replaced by

$$\frac{dM_a}{dt} = -\frac{1}{\rho}\frac{\partial p}{\partial \lambda} + \frac{\partial \overline{M_a' w'}}{\partial z}. \tag{14}$$

Thus M_a is conserved for axisymmetric frictionless flows. Note that useful interpretation requires that the coordinate system and storm axes coincide. The absolute vorticity in cylindrical coordinates is

$$\eta = \frac{1}{r}\frac{\partial rv}{\partial r} - \frac{1}{r}\frac{\partial u}{\partial \lambda} + f = \zeta + f \tag{15}$$

and in an axisymmetric vortex is related to the angular momentum through

$$\eta = \frac{1}{r}\frac{\partial M_a}{\partial r}. \tag{16}$$

Similarly, the inertia parameter is related to the angular momentum by

$$\xi = \frac{2M_a}{r^2}. \tag{17}$$

Static stability is frequently defined through the Brunt-Väisälä frequency

$$N^2 = \frac{g}{\theta_v}\frac{\partial \theta_v}{\partial z}. \tag{18}$$

Where $N^2 > 0$, the atmosphere is statically stable and vertical parcel perturbations lead to an oscillation with frequency N. For $N^2 < 0$, the atmosphere is statically unstable and vertical perturbations grow. Another measure of the static stability is the parcel buoyancy, $-g(\rho_{\text{ref}} - \rho_{\text{parcel}})/\rho_{\text{parcel}}$. Care is needed as the parcel buoyancy depends on the reference state ρ_{ref}, and while the sum of the buoyancy and perturbation-pressure[1] forces is unique, their partitioning will depend on the choice of reference state (Smith *et al.*, 2005). Note that the buoyancy vector will have a radial component (small in a tropical cyclone), as well as a vertical component.

The inertial stability

$$I^2 = \xi\eta = \frac{1}{r^3}\frac{\partial M_a^2}{\partial r} \tag{19}$$

describes the stability of the cyclone vortex to radial perturbations in an analogous manner to

[1] i.e. relative to the reference state.

that in which N^2 describes vertical perturbations. That is, radial displacements of a parcel will be strongly resisted in a region of high inertial stability, and weakly so in a region of low I. Where $I^2 > 0$, such displacements will lead to a radial oscillation of frequency I, but where $I^2 < 0$, the vortex is inertially unstable and such perturbations will grow exponentially. The inertial stability varies widely through the storm, with high stability ($I{\sim}100f$) inside of the radius of maximum winds (RMW), an abrupt decline to lower stability ($I{\sim}10f$) across the RMW followed by a gradual decline to large radii. The anticyclonic outflow layer has markedly lower inertial instability and may be inertially unstable, contributing to the marked asymmetries often found there. Inertial stability is much more variable through the storm than is static stability, and contributes to marked variations in, inter alia, the response to convective heating and the boundary layer structure. Much of the storm structure can be understood in terms of inertial stability variations.

The horizontal scale of the adjustment of the storm to added heat or momentum is governed by the relative magnitudes of the Rossby radius L_R and the forcing scale L, or by their squared ratio, the rotational Froude number $F_R = (L/L_R)^2$. The Rossby radius is defined by

$$L_R = \frac{NH}{I} \tag{20}$$

where NH is the internal gravity wave speed. Note that while it is customary to refer to *the* Rossby radius, in principle *several* radii may be relevant depending on the vertical structure of the wave, but in practice the gravest mode is the most important. The Rossby adjustment problem in dynamical meteorology studies the final steady-state energy and its partitioning between kinetic and potential components as the result of a transient or steady forcing (e.g., Gill, 1982, section 7.2). Schubert *et al.* (1980) have derived analogous results for the geostrophic adjustment of vortices on an f-plane. The details are somewhat dependent on the precise form of the forcing, but are summarised in Table 1.

Table 1. Final states in the geostrophic adjustment problem for a vortex.

Scale of forcing	Forcing	Result
Small $L \ll L_R$	Wind	Kinetic energy mostly retained, mass adjusts to balance wind field
	Mass	Most energy lost as inertia-gravity waves
Large $L \gg L_R$	Wind	Most energy lost as inertia-gravity waves
	Mass	Potential energy mostly retained, wind adjusts to balance mass field

The saturation equivalent potential temperature θ_e^* is defined as the potential temperature that a saturated air parcel would have if all its moisture was condensed out and used to warm the parcel, and may be approximated by

$$\theta_e^* \approx \theta \exp(L_v q_s / c_p T). \tag{21}$$

θ_e^* is a function of T and p only which increases with rising T and falling p; thus the highest surface values in the atmosphere occur over the warm tropical oceans in the centre of tropical cyclones. The equivalent potential temperature θ_e is defined as the θ_e^* a parcel would have if it was adiabatically expanded to saturation. Emanuel (1994, Chapter 4) gives an exact formula.

2.1. *Potential Vorticity*

"Potential vorticity thinking" has become an important tool for understanding atmospheric dynamics in recent decades. The Rossby-Ertel potential vorticity Q is defined as

$$Q = \rho^{-1} \boldsymbol{\eta} \cdot \nabla \theta \tag{22}$$

and has two properties that are crucial to this approach: (i) *conservation*: that PV is conserved for adiabatic frictionless motions, and (ii) *invertibility*: that given suitable boundary conditions and a balance relationship, the full

3-dimensional mass and wind fields can be derived from the potential vorticity distribution (Hoskins *et al.*, 1985). The importance of latent heating in tropical cyclones limits the applicability of the first property, but PV thinking has nevertheless become a cornerstone of current understanding.

The PV budget equation may be written

$$\frac{dQ}{dt} = \frac{1}{\rho}(\boldsymbol{\eta} \cdot \nabla\dot{\theta} + (\nabla \times \mathbf{F}) \cdot \nabla\theta) = \frac{1}{\rho}\nabla \cdot (\dot{\theta}\boldsymbol{\eta} + \mathbf{F} \times \nabla\theta) \quad (23)$$

respectively, with symbols defined in Table 2. In deep convection, the maximum heating typically occurs in the middle to upper troposphere. It follows that the typical effect of convective heating in a vortex is to generate cyclonic PV in the lower levels and destroy it aloft. The second equality in (23) shows that this dipole can be written as the divergence of a flux vector, $\nabla \cdot (\dot{\theta}\boldsymbol{\eta})$, hence the effect of heating may be interpreted as a transport of PV along the vorticity vector (Raymond, 1992).

A complementary view of PV dynamics was provided by Haynes and McIntyre (1987, 1990), who showed that the local change may be written as the divergence of a flux that is directed along the isentropes,

$$\frac{\partial(\sigma Q)}{\partial t} = -\nabla_\theta \cdot \mathbf{J}, \quad (24)$$

where σ is the mass density in isentropic coordinates and not a vertical coordinate. The flux $\mathbf{J}$ has components due to advection, diabatic heating and friction, which under the hydrostatic approximation[2] in isentropic coordinates are

$$\mathbf{J} = (u, v, 0)\sigma Q + (\dot{\theta}\partial v/\partial\theta, -\dot{\theta}\partial u/\partial\theta, 0) + (-F_y, F_x, 0) \quad (25)$$

with symbols defined in Table 2. This form provides a powerful constraint on the effects of heating. Since the "generation" of PV by diabatic heating can be written as a flux divergence along the isentropes, diabatic PV "generation" must be balanced by an equal and opposite "destruction" somewhere else at the same isentropic level, and heating can be interpreted as producing a purely horizontal (in isentropic coordinates) flux of PV. Haynes and McIntyre (1987, 1990) highlight two statements: (i) There can be no net transport of Rossby-Ertel PV across any isentropic surface, and (ii) PV can neither be created nor destroyed within a layer bounded by two isentropic surfaces[3]. These statements are direct consequences of (24), and "net transport", "created" and "destroyed" should be understood in that context. Finally, note that the effect of diabatic heating $\dot{\theta}$ in (24) is twofold: it produces a horizontal flux through the second term in the right-hand side of (25), and it alters the isentropic mass density σ by causing mass to cross the isentropic surfaces. However, while mass may cross the surfaces and change σ, the PV mixing ratio σQ may not. Thus if heating is causing isentropic surfaces to move together, as happens for example in the lower troposphere with convective heating maximised in the mid-troposphere, then σ will decrease. If in addition the vertical shear is small so that the diabatic heating term of $\mathbf{J}$ in (25) is small, then Q will tend to increase to compensate and thereby keep σQ constant. The opposite applies above the heating maximum. If $\mathbf{J}$ is not small, this compensating tendency will nevertheless operate in addition to the horizontal fluxes implied by (24).

3. The Secondary Circulation

The response of axisymmetric tropical cyclones in hydrostatic and gradient-wind balance to axisymmetric sources of heat $\dot{\theta}$ and momentum

[2]See Haynes and McIntyre (1987) for the nonhydrostatic version.
[3]Although net PV can be created or destroyed where the layer terminates at the ground.

F_λ is described by the Sawyer-Eliassen equation,

$$\frac{\partial}{\partial r}\left\{\frac{1}{\rho r\theta}\left[N^2\frac{\partial\psi}{\partial r}-B\frac{\partial\psi}{\partial z}\right]\right\} + \frac{\partial}{\partial z}\left\{\frac{1}{\rho r\theta}\left[\left(I^2-\frac{CB}{g}\right)\frac{\partial\psi}{\partial z}-B\frac{\partial\psi}{\partial r}\right]\right\} = g\frac{\partial(\dot\theta/\theta^2)}{\partial r}+\frac{\partial(C\dot\theta/\theta^2)}{\partial z}+\frac{\partial(\xi F_\lambda/\theta)}{\partial z}. \quad (26)$$

Here, $C \equiv v^2/r + fv$ is the radial acceleration, $B \equiv g/\theta\,\partial\theta/\partial r = \partial C/\partial z - CN^2/g$ is the baroclinicity and the equality in the definition of B is the thermal wind equation. Equation (26) describes the toroidal circulation generated by axisymmetric forcings $\dot\theta$ and F_λ, and determined also by the particular boundary conditions chosen. This toroidal circulation (u, w) is described by its streamfunction ψ, where

$$u = -\frac{1}{\rho r}\frac{\partial\psi}{\partial z}, w = \frac{1}{\rho r}\frac{\partial\psi}{\partial r}. \quad (27)$$

Equation (26) is derived in pressure-based vertical coordinates by Willoughby (1979), Shapiro and Willoughby (1982), Holland and Merrill (1984) and Willoughby (1995). Here the equation is given in height coordinates for consistency with section 2 and as it makes the surface boundary condition simpler. The principal difference is that the second term on the RHS is absent in pressure-based coordinates. Derivations in height coordinates are given by Smith *et al.* (2005) and Pendergrass and Willoughby (2009).

Equation (26) is elliptic provided that the discriminant

$$D = N^2\left(I^2-\frac{CB}{g}\right)-B^2 \quad (28)$$

is positive, a condition that Smith *et al.* (2005) show is equivalent to the potential vorticity Q being positive.

The forcings on the RHS of (26) are differentiated; thus the solution to localised forcings will consist of pairs of counter-rotating gyres. The strength and extent of these gyres will depend on the vortex structure and the boundary conditions on ψ; here the vortex structure is measured in terms of its modified inertial stability $I^2 - CB/g$, static stability N^2 and baroclinicity B. Note that (26) is linear in the forcings so that solutions obtained from individual forcings can be simply added to determine the response to the combined forcing.

The circulation induced by convective heating in the eyewall is a pair of counter-rotating gyres. The outer gyre is in an environment of weak inertial stability, so it has substantial radial extent and the motion is largely horizontal. In contrast, the inner gyre is restricted horizontally by the high inertial stability of the core and by the cylindrical geometry. Heating cannot directly change angular momentum, so the updraft between the gyres tends to be tilted to lie along a constant angular momentum surface, and hence the eyewall will tend to follow a constant M_a surface. In weak storms, the inner circulation always extends to the axis, but for $v_m \gtrsim 35\,\mathrm{m\,s^{-1}}$ the inertial stability may be sufficient to confine the circulation closer to the eyewall. These circulations produce the maximum pressure falls and tangential wind acceleration immediately inside of the eyewall, so the RMW contracts inwards as the storm intensifies. This *eyewall contraction process* has been shown to be the most common mode of cyclone intensification in the North Atlantic basin (Willoughby, 1990b). Simultaneously, the secondary circulation decelerates the flow near the storm axis, causing the radial profile of azimuthal wind to become U-shaped (Willoughby, 1978; Shapiro and Willoughby, 1982; Willoughby *et al.*, 1982). The precise details of the subsidence in the eye depend on the eye radial profile of wind: a V-shaped profile is more inertially stable inside the eye than a U-shaped, so an intense storm with a V-shaped profile has subsidence confined too close to the eyewall, while one with a U-shaped profile has subsidence extending towards the centre (Schubert *et al.*, 2007).

The surface friction-induced circulation is shallow because the static stability prevents the outflowing air from rising into the upper

troposphere. Arguments that the friction-induced circulation cannot intensify the storm (e.g., Ooyama, 1969, 1982) imply that the inwards advection of angular momentum by this circulation not exceed the frictional torque that destroys angular momentum. Balanced models are somewhat limited here as the boundary layer flow is in fact not in gradient balance (Ooyama, 1969; Smith and Montgomery, 2008) but nevertheless, more sophisticated models confirm the general structure of the induced flow and that the net angular momentum import and frictional torque nearly balance (Kepert and Wang 2001; see also section 5.1.2).

Momentum forcing in the upper troposphere induces a shallow, radially extensive pair of gyres, because of the weak inertial stability there. This forcing is important to understanding the interactions between the cyclone and its environment, since upper troughs may induce an eddy flux convergence of angular momentum in the upper part of the storm.

Numerous authors have given the details of the secondary circulation in particular situations, including Willoughby (1979, 1990b), Pfeffer and Challa (1981, 1992), Shapiro and Willoughby (1982), Holland and Merrill (1984) and Pendergrass and Willoughby (2009).

3.1. *Cooperative Intensification*

These responses of the secondary circulation to the various forcings provide a framework for understanding the energetics of the tropical cyclone as a whole. The boundary layer circulation can only spin down the storm, since the inwards advection of angular momentum by the frictional inflow is countered by the surface frictional torque and by outwards advection in the return branch of the gyre. Indeed, this outflow spins down a storm in a matter of days (Eliassen and Lystad, 1977; Montgomery *et al.*, 2001; Reasor *et al.*, 2000). Nor can surface friction lift surface air to the upper tropospheric outflow channel against atmospheric stability. However, it does define a radius inside of which there is frictionally forced ascent of warm moist air out of the boundary layer. While this air is too cool to overcome the basic stability gradient, release of latent heat allows the air to ascend higher. This latent heat release in and surrounding the eyewall induces a much deeper secondary circulation, with weak inflow through much of the troposphere and outflow just below the tropopause. The low–mid tropospheric inflow induced by the heating is sufficient to cancel the outflow component of the frictionally-forced circulation in balanced models[4], at least in intensifying and steady-state storms, producing the observed deep weak inflow in the mid troposphere in real storms. The role of boundary-layer convergence in defining the regions of deep ascent is supported by observations showing that the vertical mass flux is maximised near 1-km altitude in the eyewall, rainband and stratiform rain regions (Black *et al.*, 1996).

As the primary circulation intensifies, the inertial stability of the core increases, which modifies the character of the secondary circulation. The boundary between frictionally-forced upflow and downflow migrates inwards, confining the latent heating to be closer to the centre and increasing the efficiency by which heating spins up the storm (Hack and Schubert, 1986). The heating-induced secondary circulation also contracts and strengthens the downdraft in the eye. There is thus a cooperative interaction between the primary and secondary circulations in an intensifying storm, first discussed in detail by Ooyama (1969) in the context of a 3-layer balanced model and further elicudated by Ooyama (1982). Note that this feedback implies that tropical cyclone intensification and maintenance is inherently a nonlinear process. While the Sawyer-Eliassen equation (26) is linear in the forcings, tropical cyclone intensification is nonlinear because, inter alia, the friction-induced

[4]But not the thin layer of outflow above the boundary layer due to the readjustment of supergradient flow, as discussed in section 5.

circulation defines the regions favourable for deep convection.

The intensification is eventually limited as the increase in strength of the upper warm core increases the static stability and limits the ability of the upflowing boundary layer air to ascend. Then the azimuthal-mean updraft becomes moist neutral to the ascent along the slanting angular momentum surfaces. This limit is assumed by Emanuel's potential intensity theory (section 4). We shall see later that other processes, such as the formation of secondary wind maxima and instabilities of the eyewall itself, may also act to limit the intensification.

How important is the assumption of thermal wind balance in the above arguments? For quantitative prediction, the requirement of balance is a significant limitation and the theory is only strictly valid for weak forcings and slow secondary circulations. In much of the boundary layer, the flow is significantly subgradient, with the lack of balance there recognised as a serious limitation of balanced models as far back as Ooyama (1969). However, the more sophisticated boundary layer models discussed in section 5 do qualitatively reproduce the main features of the balance model: a strong near-surface inflow layer with ascent up out of the boundary layer in the core, and subsidence into the boundary layer at larger radii. Above the boundary layer, analyses of observations confirm gradient balance to within 1 or $2\,\mathrm{m\,s^{-1}}$ (Willoughby, 1990a, 1991; Kepert, 2006a,b), although one modelling study suggested a thin annulus of supergradient flow on the inner edge of the eyewall (Zhang *et al.*, 2001). Overall, the evidence largely supports the balance assumption in this part of the storm and the cooperative intensification analysis is therefore reasonable.

From this perspective, what is the role of deep convection in a tropical cyclone[5]? Its horizontal location is largely defined by the region of frictionally-forced ascent. Thus the most obvious impact is that it determines the vertical profile of heating, thereby affecting the structure of the secondary circulation. The secondary circulation in a real tropical cyclone is not the spatially-smooth field suggested by the solution of the Sawyer-Eliassen equation, but rather a substantial proportion ($\sim$ 65%) of the total upwards transport in the eyewall and in rainbands is concentrated into buoyant updraft cores that occupy a small ($< 10\%$) of the area of each region. Most of the updraft cores are positively buoyant, and these accomplish about 40% of the total transport, but occupy $< 5\%$ of the total area. These statistics are from Eastin *et al.* (2005a,b), but similar results were found from observational analyses by Jorgensen *et al.* (1985) and Black *et al.* (1996)), and from high-resolution modelling by Braun (2002), Braun *et al.* (2006) and Cram *et al.* (2007). Ooyama (1982) argues that buoyant energy release is necessary since it enables midtropospheric entrainment in the cloud bands and hence causes the deep inflow that imports angular momentum to intensify the vortex. The upwards transport from these updrafts is partially opposed by downdraft cores which, as we shall see in section 5, act to cool and dry the boundary layer. If there were no surface fluxes, these downdrafts would reduce or eliminate the ability of the air flowing up and out of the boundary layer to overcome the stability gradient and ascend to the tropopause. Over the warm tropical oceans, the thermodynamic fluxes that enable the recovery of the boundary layer from these downdrafts are thus crucial to maintenance of the storm. Following landfall, these fluxes are greatly reduced and significant outflow may be observed above the boundary layer, consistent with the collapse of the latent-heat induced part of the secondary circulation and also with the increased frictional forcing.

[5]Note that nonprecipitating clouds do not provide net heating since their evaporation consumes the latent heat released by their formation, although they do generate some vertical transport.

3.2. *Eyewall Replacement Cycles*

Convective rings other than the eyewall may also occur in tropical cyclones, particularly intense ones. Such rings will generate a secondary circulation consisting of a pair of gyres similar to that generated by the eyewall heating, although the precise details will differ because of differing inertial and static stabilities and baroclinicity at the larger radius. In intense hurricanes ($v_m \gtrsim 50\,\mathrm{m\,s^{-1}}$), the appearance of an outer eyewall or concentric ring usually marks the end of the period of intensification, and possibly a weakening of the storm. This occurs because the secondary circulation of the outer ring competes with the eyewall and its wind maximum by two mechanisms. Firstly, the outer ring's secondary circulation produces broad subsidence over the eyewall and hence surface divergence and outflow there, which acts directly to weaken the inner wind maximum (Willoughby *et al.*, 1982). Secondly, the convection in the outer ring consumes high-enthalpy air from the inflowing boundary layer and frequently replaces it with cool dry downdrafts (section 7.1), thus shutting off part of the energy supply to the eyewall. Often, these processes lead to the destruction of the inner eyewall and its wind maximum. The outer ring then becomes the main eyewall and intensification may resume as it contracts. This sequence of events is known as the eyewall replacement cycle, and intense storms may undergo several such cycles. Detailed case studies may be found in Willoughby *et al.* (1982), Willoughby (1990a) and Willoughby (1995), while a satellite view of the sequence is shown in Chapter 7.

The above mechanism describes the evolution once the convective ring has formed, but is silent on the question of where the ring comes from. Time-sequence imagery from microwave satellite sensors or radar suggest that the "wrapping-up" of a spiral rainband is a common route, but does not reveal the underlying dynamics. Experiments with barotropic models have shown that the interaction between a small intense vortex and a large weaker one may lead to the smaller vortex straining out the larger one into an annulus of elevated vorticity surrounding the smaller vortex, with a moat of low vorticity in between (Kuo *et al.*, 2004). In velocity space, this configuration corresponds to an outer wind maximum. Other outcomes are possible from this interaction, and this scenario depends on a certain range of initial vortex sizes, relative intensities and separations. Rozoff *et al.* (2006) have shown that the strong radial shear in the moat between the concentric eyewalls leads to rapid filamentation which they hypothesise acts to suppress convection there in conjunction with the subsidence forced by the respective secondary circulations. However, Wang (2008) has shown that the filamentation zone, instead of suppressing deep convection, actually provides a favourable environment for organising inner spiral rainbands, and that the low-reflectivity moat outside the eyewall is primarily controlled by subsidence from the secondary circulation and from downdrafts from anvil precipitation outside of the eyewall. In contrast, Nong and Emanuel (2003) have shown using an axisymmetric model that a WISHE-like instability (see section 4) may strengthen an existing outer local wind maximum, although this mechanism cannot explain the initial origins of the finite-amplitude instability. Terwey and Montgomery (2008) propose a hypothesis for secondary eyewall formation which includes the WISHE process, and in which the necessary wind maximum is generated by a combination of convective scale, vortex Rossby wave (section 7.2) scale and system scale processes. Further research is clearly needed to understand the formation mechanism(s) of secondary eyewalls, and is a requirement for improved intensity forecasts.

3.3. *The Outflow Layer*

The outflow layer consists of a small cyclonic core surrounded by an extensive asymmetric anticyclone. It is easy to understand why the flow should turn anticyclonic: M_a is destroyed

in the frictional inflow layer but approximately conserved in the eyewall updraft and outflow, hence the outflow must have lower M_a than lower in the storm at the same radius, eventually to the extent that the flow turns anticyclonic. However, some studies of the upper troposphere surrounding a cyclone reveal areas of anticyclonic PV (e.g., Molinari *et al.*, 1998; Shapiro and Franklin, 1995; Wu and Cheng, 1999), as shown in Fig. 1. A similar feature occurs in idealised numerical simulations (e.g., Shapiro, 1992). The simple argument using M_a is deficient in that it cannot explain the sign change of η that apparently occurs. Similarly, advective rearrangement in adiabatic frictionless PV dynamics cannot create PV of the opposite sign. Shapiro (1992) shows that the upper-level negative PV was generated in his model by twisting terms that arise from horizontal gradients of the cumulus mass flux. A further clue to the dynamics can be found in the Haynes and McIntyre (1987) form of the PV budget equation, (24). The isentropic surfaces in the outflow layer bend downwards into the mid troposphere in the storm core, because the core is warm. If convective processes are leading to an increase in low- and mid-tropospheric PV at the core, there must be a compensating decrease elsewhere at the same isentropic level. It is plausible, although not yet established in this framework, to hypothesise that this decrease may be sufficient to lead to locally anticyclonic PV adjacent to the storm. The Haynes and McIntyre form of the PV budget equation shows that such behaviour should not be regarded as being anomalous but rather, as consistent with the generation of strong cyclonic PV in the core of the intensifying storm. Examination of Fig. 1 as well as the full sequence from which it came (Wu and Cheng, 1999) tends to support the idea that the upper anticyclonic PV develops in conjunction with intensification of the cyclone core.

The outflow layer is thus inertially either weakly stable or unstable. This contrasts markedly with the rest of the storm and has at least two important consequences. Firstly, it is much less symmetric than the lower part of the storm, with the outflow being often organised

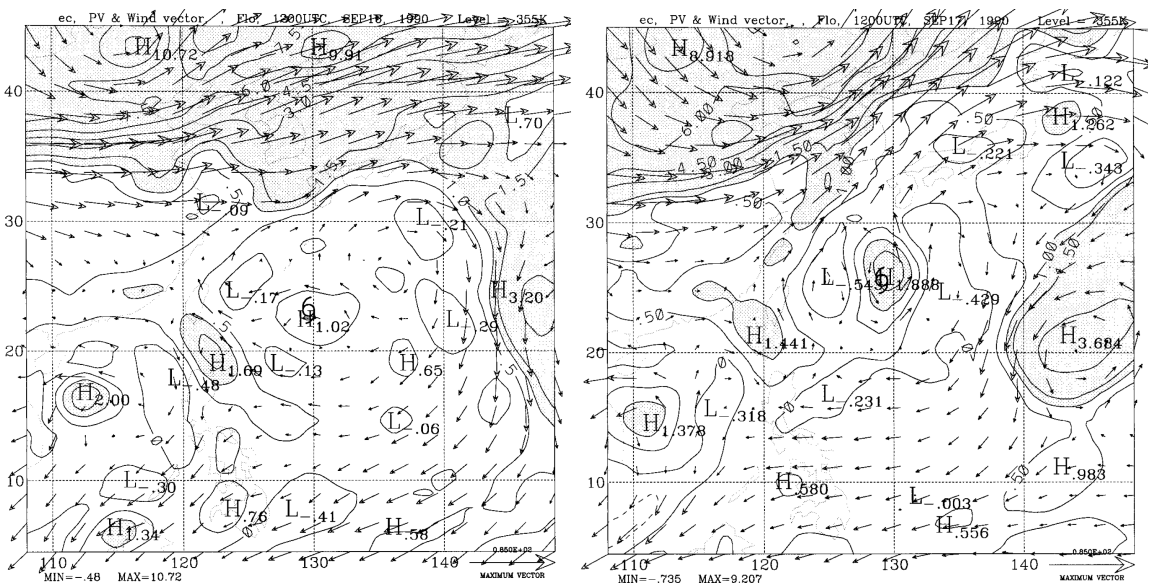

Figure 1. Wind vectors and PV on the $\theta = 355$ K surface at (left) 1200UTC 16 Sep and (right) 1200UTC 17 Sep 1990 during SuperTyphoon Flo. PV contoured every 0.5 PVU up to 1.5 PVU and every 1.5 PVU thereafter, with values greater than 1 PVU shaded. Note the development of anticyclonic PV surrounding the core, as the core intensified. From Wu and Cheng (1999).

into one or two jets. These may form through inertial instability, but in any case, low inertial stability favours the outflow of the air exhausted from the eyewall convection and hence intensification. Secondly, the low inertial instability provides a conduit through which the environment can directly influence the storm core. In the upper troposphere, the storm core is not protected by an annulus of inertially stable air as in the lower troposphere. Moreover, the low stability ensures that environmental forcing will produce a marked radial-flow response. We will see in section 8 that upper tropospheric interactions between the cyclone and its environment can have a major effect on the storm's evolution.

4. Potential Intensity Theories

Potential intensity (PI) theories attempt to answer the question: What is the maximum equilibrium intensity that a tropical cyclone can reach in a given thermodynamic environment? Here we review two branches of theory: Holland (1997) and predecessors calculate the surface pressure drop realisable by convective heating, while Emanuel's (Emanuel, 1986, 1988, 1995; Bister and Emanuel, 1998) balances the rate of extraction of enthalpy from the sea surface against frictional destruction of kinetic energy.

Emanuel's PI theory (EPI) makes an analogy with the Carnot cycle, in which the cyclone's secondary circulation contains the classical Carnot-cycle elements of isothermal expansion of the inflowing boundary layer air, adiabatic expansion as it ascends in the eyewall and flows outwards in the upper troposphere, isothermal compression at large radius and descent back to the boundary layer. Although the analogy is not exact (since the outer part of the cycle is not closed in real tropical cyclones), an important consequence is that the efficiency of the tropical cyclone as a heat engine can be calculated. Multiplying this efficiency by the surface enthalpy gain gives the amount of work the cyclone can do. Assuming that all of this work is expended in frictional dissipation leads to Emanuel's expression for the potential intensity,

$$v_m^2 = \frac{T_s - T_o}{T_o} \frac{C_E}{C_D} (k_0^* - k) \qquad (29)$$

The full derivation can be found in Bister and Emanuel (1998) and a simplified version in Emanuel (2003).

The EPI model consists of two components, the boundary layer and the rest of the cyclone. The former is represented by a linearised depth-averaged model, whose role is to determine the dynamical and thermodynamical properties of the frictionally forced updraft near the RMW. The role of the surface enthalpy fluxes in making the expansion of the inflowing boundary layer air isothermal rather than adiabatic is emphasised in this part of the model through the acronym WISHE, for wind-induced surface heat exchange. The remainder of the model includes the important assumption that the cyclone core is neutral to moist slantwise convection; that is, that the θ_e^* and angular momentum surfaces coincide. This assumption amounts to a convection parameterisation because it determines how the effects of the latent heating are distributed in the rest of the cyclone, given the boundary layer updraft properties (Smith, 2000). EPI theory can thus be regarded as a steady-state version of the cooperative intensification theory discussed in section 3.1, in which the neutrality to moist convection (i) is consistent with the cyclone having reached peak intensity as it implies that there is just sufficient latent heat release to allow the boundary layer air to ascend, but not enough to intensify the storm further, and (ii) enables an analytical solution for the intensity of the storm.

Equation (29) shows that the EPI depends upon the ratio C_E/C_D of the surface enthalpy and drag coefficients. Similar results have been obtained by prognostic tropical cyclone models, with Ooyama (1969) and Rosenthal (1971) being the first to identify the importance of this ratio. Measurements generally show that C_E is nearly constant with wind speed, while C_D was long

thought to increase linearly with wind speed. The resulting decrease in the ratio at high winds was an obstacle for EPI theory. This difficulty has apparently been removed by recent measurements showing that C_D ceases to increase, and in fact may decrease, once the wind speed exceeds about $35\,\mathrm{m\,s^{-1}}$ (Chapter 3).

Persing and Montgomery (2003) used an axisymmetric model to test EPI theory. They found that, when run at high resolution, the model predicted intensity averaging about $40\,\mathrm{m\,s^{-1}}$ higher than the EPI, a phenomenon they dubbed "superintensity". They argued that superintensity occurred when the model developed small-scale streamwise vortices along the inner edge of the eyewall, which efficiently mixed the high θ_e air from the eye boundary layer into the eyewall updraft, increasing the energy content of this air and hence the storm intensity. The low-level air within the eye has high values of θ_e since it has been in contact with the warm ocean surface at lower pressure than that beneath the eyewall. However, Bryan and Rotunno (2009a) presented simulations in which this mechanism was removed by artificially setting the surface moisture fluxes in the eye to zero, and showed that this change had only a negligibly small impact on intensity. Bryan and Rotunno (2009b) further demonstrated that the simulated intensity in an axisymmetric model has a strong sensitivity to the parameterisation of horizontal diffusion, and showed that the incorrect representation of this process was responsible for the results of Persing and Montgomery (2003). While entrainment of the eye reservoir of high θ_e air does not explain superintensity of the axisymmetric mean vortex, numerical (Braun, 2002; Cram *et al.*, 2007) and observational (Eastin *et al.*, 2005a,b) evidence suggests that it may be important to the development of individual buoyant updrafts on shorter timescales.

Observational comparisons tend to show that EPI is an upper bound to observed intensity (e.g., Emanuel, 2000; Tonkin *et al.*, 2000). A notable exception is an analysis of Hurricane Isabel (2002) based on dropsonde data, in which the intensity substantially exceeded the EPI (Montgomery *et al.*, 2006).

In contrast to EPI, the Holland (1997) PI theory (HPI) calculates the hydrostatic pressure fall resulting from the vertical redistribution of moist entropy obtained at the sea surface. The model defines an eyewall saturation moist adiabat whose θ_e^* is set by the surface conditions, surrounding a parameterised eye. The model thus contains an explicit feedback, since reduced hydrostatic pressure increases the surface θ_e^* (section 2) and hence energy available. Unlike EPI theory, HPI does not explicitly incorporate an energy budget, although an energy balance is used to exclude certain unrealistic occurrences. Boundary layer processes are included implicitly since the thermodynamics of the ascending air depends on the SST, prescribed boundary-layer humidity and surface pressure, but there is no explicit boundary-layer submodel. Holland (1997) assumes that the ascending air's θ_e^* is determined by the surface conditions beneath the eyewall, but discusses the possibility of higher intensity if some process acted to transfer the higher-θ_e^* air from the eye boundary layer into the eyewall updraft.

While these theories produce similar predictions for typical tropical environments and are reasonably consistent with observations, they are fundamentally different in approach and make some significantly different predictions. For example, they have opposite sensitivities to the assumed boundary layer relative humidity: Emanuel's theory predicts the strongest storms for low RH because that maximises the surface enthalpy flux, while Holland's predicts the strongest storms for large RH since that maximises the eyewall θ_e^*. This and other differences between the theories are detailed in Camp and Montgomery (2001).

The Emanuel and Holland PI theories, and indeed many numerical simulations of tropical cyclones, assume axisymmetry. Bryan and Rotunno (2009b) have examined the sensitivity of such simulations to various parameterisations

in the model, including the horizontal diffusion, the hydrometeor fall velocity, and the ratio C_E/C_D. They found that intensity was strongly sensitive to each of these factors, and also that the magnitude of sensitivity of the latter two factors was quite dependent on the horizontal diffusion. In an axisymmetric model, the horizontal diffusion represents a range of asymmetric mixing processes, including eyewall mesovortices, vortex Rossby waves and boundary layer roll vortices as well as turbulence. It affects the simulated intensity by controlling the degree to which frontogenesis can collapse the eyewall to a singularity (Emanuel, 1997). Bryan and Rotunno (2009b) argue for sufficiently large horizontal diffusivity in axisymmetric models as to have a significant impact on the simulated intensity, and note that such values substantially reduce the sensitivity of intensity to the ratio C_E/C_D, from that in earlier studies.

Tropical cyclones intensify at a finite rate and thus require time to achieve their potential intensity. Factors such as the favourability of the environment determine how quickly, and whether, they get there. Indeed, the majority of storms do not reach their PI. Emanuel (2000) studied the frequency distribution of storm relative intensity; that is, peak intensity normalised by the potential intensity at the same time. He showed that the frequency distribution of relative intensity for storms whose intensity was not limited by landfall or transition over colder water could be modelled as the combination of two uniform distributions, with all normalised intensities from zero (marginal tropical cyclone) to hurricane intensity being about equally likely, then a step to another near-constant probability for all storms from hurricane intensity to a normalised intensity of one (i.e. a storm at its PI). In particular, it is relatively rare for a storm to attain its PI.

An earlier theory of hurricane intensification was known as CISK, for conditional instability of the second kind. The linear CISK theory of Charney and Eliassen (1964) differs substantially from the above theories, because it is fuelled by pre-existing atmospheric conditional instability rather than by enthalpy drawn from the sea beneath the storm. Ooyama's similar (1964) theory later matured into his nonlinear cooperative-intensification theory (Ooyama, 1969, 1982), presented in section 3.1 in the context of a continuous balanced-vortex model rather than his 3-layer model. Smith (1997) compares these models in detail, and concludes that the differences between EPI theory and Ooyama's cooperative intensification are largely restricted to technical details and degrees of emphasis on the relative importance of surface fluxes. Importantly, and in contrast to Charney and Eliassen (1964), cooperative intensification and EPI agree that both surface fluxes and convection are necessary for intensification.

5. Boundary Layer Structure

Boundary layer processes determine the supply of thermodynamic energy to the storm and the dissipation of momentum through friction, processes that we have seen are crucial to the storm's existence. In addition, it is through the boundary layer that much of the impact on humanity occurs. Recent observational and theoretical advances have led to substantial progress on understanding this part of the storm.

5.1. *Mean Structure*

5.1.1. *Observations*

Observed wind profiles in tropical cyclones frequently show a marked low level wind maximum. This maximum typically occurs around 300 to 800 m height near the eyewall, and 1 to 2 km at larger radius. It has been observed by dropsonde (Franklin *et al.*, 2003; Kepert, 2006a,b), wind profiler (e.g., Knupp *et al.*, 2000, 2005), and Doppler radar (e.g., Marks *et al.*, 1999), although it has been the recent advent of the GPS dropsonde that has emphasised the ubiquity of this

jet. The broad maximum is generally more or less obscured by smaller-scale fluctuations due to turbulence in individual soundings, thus some form of averaging is needed to expose it clearly. For example, Fig. 2 shows the observed mean wind speed profile, normalised by the wind speed at the common aircraft flight level of 700 hPa or about 3 km, from the eyewall of seven hurricanes. The low level jet is clearly apparent. Below the jet, in the lowest 100–200 m, the wind speed increases nearly logarithmically with height (Franklin *et al.*, 2003; Powell *et al.*, 2003), consistent with classical theory for a neutrally-stratified surface layer.

A substantial amount of between-storm variability is apparent in Fig. 2. The strength of the normalised maximum varies from 1.12 to 1.3, and its height from 300 to 800 m, while the strength of the normalised surface wind speed is between 0.82 and 0.96.

Along with variation between storms, there is substantial variation within each storm. The decrease in height of the low-level jet with decreasing radius becomes quite marked across the eyewall, and continues to the centre of the storm (Franklin *et al.*, 2003; Kepert, 2006a,b). Figure 3 shows the observed mean storm-relative wind profile in several annular regions in Hurricane Mitch (1998); it is clear that the depth of the frictional inflow layer and the jet height decrease towards the centre. Moreover, the azimuthal-wind maximum is generally near the top of, but still within, the frictional inflow layer. Within the eye itself, both individual and mean soundings generally show little, if any, evidence of frictional retardation at the surface.

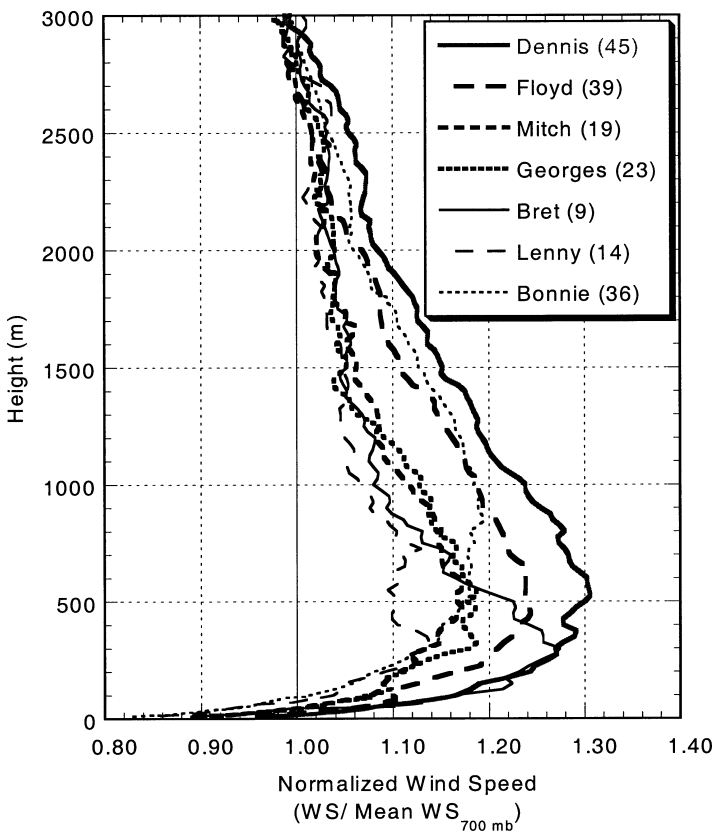

Figure 2. Mean observed eyewall wind speed profile in seven hurricanes, normalised by the wind speed at 700 hPa. From Franklin *et al.* (2003).

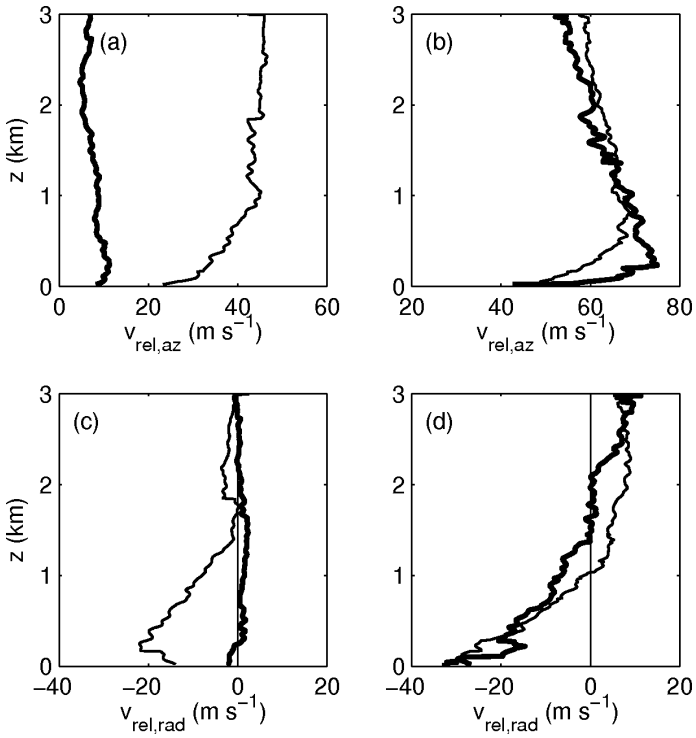

Figure 3. Observed wind profiles in Hurricane Mitch (1998). (a) Mean profiles of storm-relative azimuthal wind over radius ranges 0–15 km (heavy) and 40–100 km (light). (b) As for (a) except over radius ranges 15–25 km (heavy) and 25–40 km (light). (c, d) As for (a, b), but for the storm-relative radial wind component. From Kepert (2006b).

This radial variation in wind structure is accompanied by a variation in the surface wind factor (SWF); that is, the ratio of the near-surface wind speed to that at some higher level. Franklin *et al.* (2003) showed that the hitherto widely used value of 0.8 is appropriate for the outer vortex, but increases to 0.9 near the eyewall. They also found that the SWF varied with reference height, recommended higher values in the outer vortex near convection than in its absence, and noted higher values on the left of the storm track than on the right. These new values revised long-standing operational practice at the United States National Hurricane Center.

The SWF has been analysed in individual storms by Kepert (2006a,b) and Schwendike and Kepert (2008). The increase towards the storm centre is clearly marked, and most storms display higher values on the left of track than on the right. However other factors, including proximity to land in the case of Hurricane Mitch (1998), can also produce a significant SWF asymmetry. Surface wind data from the airborne step-frequency microwave radiometer (SFMR) usually shows an increase in SWF towards the centre, and often a left-right asymmetry as well (Powell *et al.*, 2009).

There is also a marked azimuthal variation in tropical cyclone boundary layer wind structure. Figure 4 shows the observed profiles in Hurricane Georges (1998). It is clear that a large part of the variability between profiles is due to their position within the storm (Kepert, 2006a,b); this relationship is especially striking as observations nearby in storm-relative space are not necessarily nearby in time. The height and strength of the low-level jet, and the depth and strength of the inflow layer, vary consistently around the storm. Analyses of Hurricanes Mitch (Kepert, 2006b),

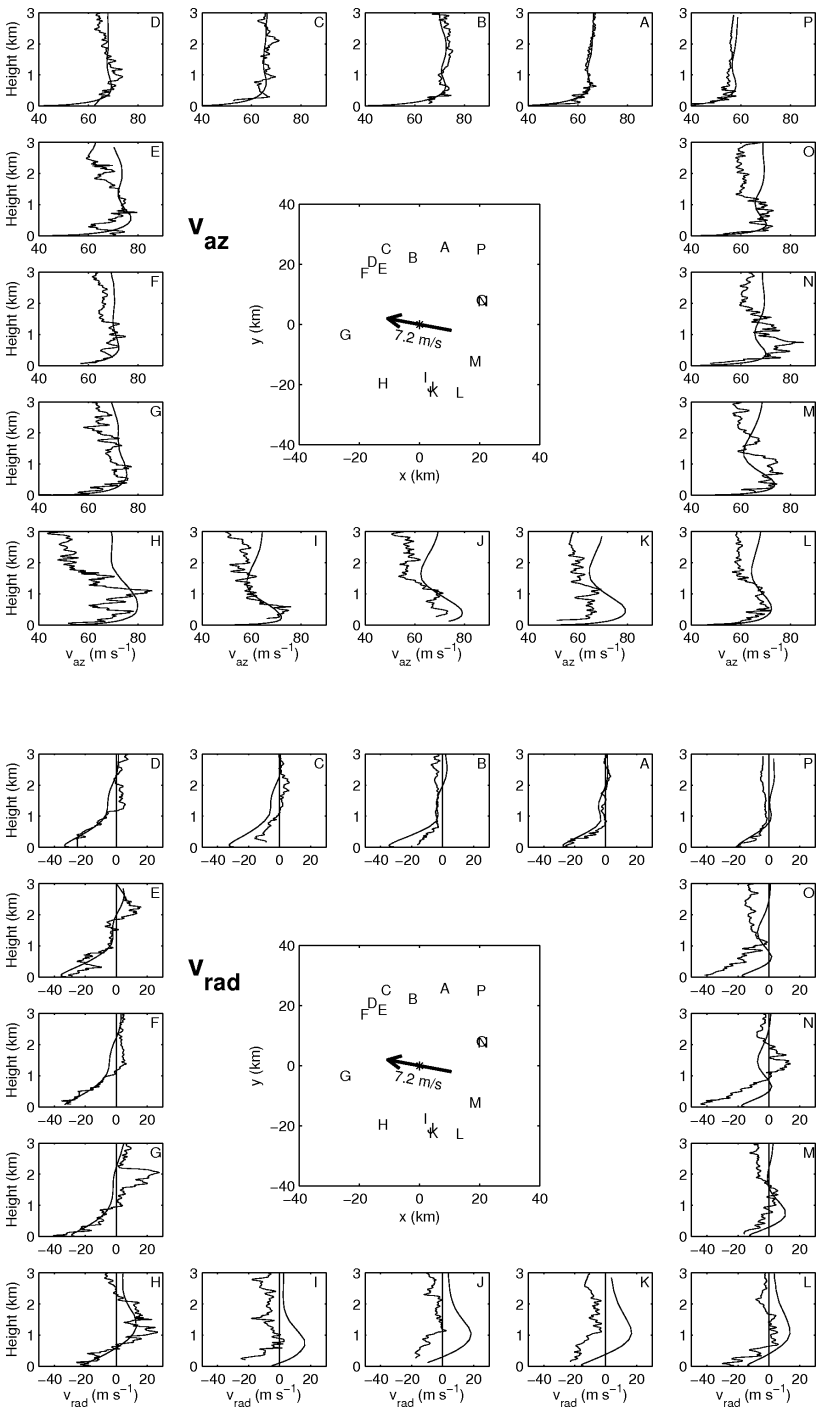

Figure 4. Profiles of the storm-relative azimuthal and radial wind components observed by dropsondes (curves with small-scale fluctuations) and represented in the model of Kepert and Wang (2001) (smooth curves) in and near the eyewall of Hurricane Georges (1998). The model values were interpolated from the model grid to the observed dropsonde trajectory. The storm-relative position of each sonde as it fell through a height of 1 km and the storm motion are shown in the central panel. From Kepert (2006a).

Danielle and Isabel (Schwendike and Kepert, 2008; Bell and Montgomery, 2008) similarly show a consistent spatial variation of wind profile shape within each storm.

The strongest surface winds are generally found in the right forward quadrant in the northern hemisphere, although exceptions to this situation are not uncommon. The rightward location can be understood to first order as the sum of the motion vector and the symmetric storm circulation. Maximum earth-relative inflow occurs to the right rear, with weaker or absent inflow to the left. The net surface wind asymmetry is thus roughly a right-rear to left-front throughflow (e.g., Powell, 1982; Black *et al.*, 1988; Powell and Houston, 1998; Kepert, 2006a).

Several of the theoretical studies reviewed below have predicted that the upper boundary layer jet is supergradient. Balance in this situation has been analysed by Kepert (2006a), Kepert (2006b), Schwendike and Kepert (2008) and Bell and Montgomery (2008), who found that Hurricanes Mitch (1998) and Isabel (2002) had azimuthal-mean jets that were ∼15% supergradient, but that Georges (1998) and Danielle (1998) did not. These differences highlight the inter-storm variatiability already described, and are discussed further below.

Several studies have discussed boundary layer asymmetries due to proximity to land. Here, the higher roughness over land induces increased inflow, which is typically drier, and produces a flow asymmetry that may extend into the eyewall. Analyses of these phenomena have been presented for Hurricanes Bonnie (Schneider and Barnes, 2005), Danny (Kepert, 2002a), Floyd (Kepert, 2002b) and Mitch (Kepert, 2006b). Simulation with simplified models shows that the cause of the flow asymmetry is asymmetric friction, analogous to that produced by storm motion (Kepert, 2006b; Wong and Chan, 2007; May *et al.*, 2008).

Boundary-layer thermodynamics was analysed along inflow trajectories in Hurricane Bonnie (1998) by Wroe and Barnes (2003). They found little increase in inflow θ_e to within about 1.5 times the RMW, despite surface fluxes of over 500 $\mathrm{W\,m^{-2}}$, since moist convection removes energy from the boundary layer at the same rate as the sea supplies it. Inwards of this, the storm's secondary circulation suppresses convection while the surface fluxes continue to increase, giving an increase in θ_e. This structure is consistent with observations showing an annulus of increased sea–air temperature contrast and reduced humidity somewhat outside of the RMW (Cione *et al.*, 2000; Barnes and Bogner, 2001). To achieve energy balance, Wroe and Barnes (2003) found it was necessary to either allow for some entrainment through the boundary layer top, or for turbulence dissipative heating. The energetics of the boundary layer are of prime importance, in light of the considerable sensitivity of storm intensity to the energy content of the boundary layer air beneath the eyewall seen in section 4. The impact of spiral band convection on boundary layer thermodynamics is discussed further in section 7.

5.1.2. *Theory and Modelling*

A satisfactory theory of the tropical cyclone boundary layer is thus challenged to explain the rich observed structure variation between storms, and with radius and azimuth within individual storms. Idealised models of the tropical cyclone boundary layer date back to the 1960s and beyond, and may be classified by their dimension:

- *1-D column:* Moss and Rosenthal (1975); Powell (1980).
- *1-D depth-averaged axisymmetric:* Smith (1968, 2003); Smith and Montgomery (2008); Smith and Vogl (2008).
- *2-D axisymmetric:* Rosenthal (1962); Carrier (1971); Eliassen (1971); Kuo (1971, 1982); Eliassen and Lystad (1977); Mallett (2000); Montgomery *et al.* (2001).
- *2-D depth-averaged:* Shapiro (1983); Vickery *et al.* (2000).
- *3-D:* Kepert (2001); Kepert and Wang (2001).

The calculated flow from several of the 2-D axisymmetric models, and from the 3-D models, display upper boundary layer wind maxima. These simulations have much in common with the observations; the azimuthal maximum is contained within the frictional inflow layer, the maximum becomes more marked towards the centre of the storm, and the depth of the boundary layer decreases towards the centre of the storm. This last property is because the boundary layer has high Rossby-number Ekman layer scaling such that the depth varies inversely with the square root of the inertial stability (Rosenthal, 1962; Eliassen and Lystad, 1977; Kepert, 2001). Indeed, these studies showed that the tropical cyclone boundary layer is a modified Ekman spiral, in which the inertial stability parameter I replaces the Coriolis parameter f, and the spiral is "stretched" in the cross-stream direction by a factor $(\xi/\eta)^{1/2}$. The upper boundary layer wind maximum is similar to that in the Ekman spiral, and a few percent supergradient in these simple models.

These simpler models ignore the influence of vertical advection; including this process gives a markedly more supergradient wind maximum. Analysis of the momentum budget equations shows that the supergradient flow is generated by inwards advection of angular momentum. The inflow is ultimately frictionally generated, but is maintained at the jet height against the outwards acceleration due to gradient imbalance by diffusive and advective transport from below; thus it is stronger in a model that contains vertical advection (Kepert and Wang, 2001). Kepert (2006b) further relates this effect to a modification of the Ekman-like solution as follows: if the vertical advection is zero or neglected, the oscillation and decay length-scales in the Ekman-like solution are equal. Introducing vertical advection makes these scales unequal; in an updraft, the oscillation scale is longer than that for decay, while in a downdraft the opposite applies. Thus the flow will exhibit larger oscillations with height near the boundary layer top in an updraft than in a downdraft. This effect is strongest where upwards motion is strongest, so the boundary layer jet is most marked beneath the eyewall and near rainbands, as is also apparent in the models of Kuo (1971, 1982).

The height-resolving 2-D and 3-D models generally show an increase in the SWF towards the centre of the storm. The depth-averaged axisymmetric and 2-D models show a similar increase in the relative strength of the boundary layer mean wind towards the centre. In both cases, this is due to advection of angular momentum by the frictional inflow maintaining relatively stronger near-surface winds than in boundary layers with straight flow, and the effect is strongest where both the inflow and radial gradient of angular momentum are strong; that is, near the eyewall and possibly also near updrafts associated with secondary wind maxima in outer convective rings. It is important to note that these models do not include any enhancement of the turbulent transport by moist convection; thus the effect is purely dynamical.

Having established that radial advection plays an important role in shaping the structure of the axisymmetric boundary layer, it is perhaps not surprising to learn that azimuthal advection also has a strong influence. Kepert (2001) showed that the motion-induced asymmetry has the horizontal structure of a wavenumber-1 inertia wave. Such waves normally propagate, with the phase speed varying rapidly with radius and are not observed. However, the effect of vertical diffusion is to retard the wave propagation: both the vertical tilt (in azimuth) of the phase lines and the decay of the wave amplitude adjust so as to bring the wave to a halt, locked in position with the asymmetric friction forcing it at the surface. There are two such waves, corresponding to the anticyclonically- and cyclonically-propagating inertia waves, but the stalled version of the anticyclonically-propagating one dominates. It rotates anticyclonically with increasing height, and has a

depth scale several times that of the symmetric component. The inclusion of nonlinear processes, including vertical advection, tends to strengthen the asymmetric flow over that predicted by the linear analysis (Kepert and Wang, 2001). Analysis of dropsonde observations in Hurricanes Georges, Mitch and Danielle, but not Isabel, clearly show the predicted anticyclonic rotation of the phase of the asymmetry with height (Kepert, 2006a,b; Schwendike and Kepert, 2008).

This stalled wave structure, when combined with the symmetric component, is able to explain several well-known features of the tropical cyclone boundary layer. In the northern hemisphere, the surface earth-relative wind maximum is in the right forward quadrant, and the inflow angles are greatest on the right of track and least on the left. It also predicts the more recent observational findings, including that the boundary layer jet is more marked, more strongly supergradient, and closer to the surface on the left of track, and that the SWF is higher on the left than on the right. These higher-dimension models demonstrate an important fact: that the boundary layer of a tropical cyclone is distinct from that in much of the rest of the atmosphere, and cannot be satisfactorily understood by 1-D models that assume horizontally homogeneity. Rather, radial advection of angular momentum by the frictional inflow and asymmetric frictional forcing play a substantial role in determining the boundary layer structure and depth.

Variations in angular momentum advection play an important role in determining the spatial variation in tropical cyclone boundary layer wind profile structure. The radial gradient in angular momentum varies greatly between storms — some storms have relatively "flat" radial variation in the wind strength, or equivalently, are inertially stable and have a strong radial gradient of angular momentum throughout, while others have "peaked" profiles, and are inertially near-neutral with a relatively weak angular momentum gradient outside the RMW. Kepert and Wang (2001) presented model calculations of the resulting boundary layer structure for these extremes. The "flat" case had a weakly (5–10%) supergradient jet extending from the RMW to large radii, while the "peaked" one had a strongly (25%) supergradient jet confined to the vicinity of the RMW. The frictional inflow and eyewall updraft are also relatively stronger in the "peaked" case. Observational confirmation of these differences has been provided by Kepert (2006a,b), Bell and Montgomery (2008) and Schwendike and Kepert (2008), who found that of four storms analysed (Danielle, Georges and Mitch of 1998, and Isabel of 2002), two had markedly supergradient flow in the upper boundary layer beneath the eyewall, and two were indistinguishable from balance. The difference in the structure of these storms is as predicted by Kepert and Wang (2001): the "peaked" storms had supergradient flow, while the "flat" ones did not. Figure 4 illustrates the modelled wind profiles in Hurricane Georges corresponding to the dropsonde observations, and shows that the model is able to reproduce much of the around-storm variation in structure, in both the azimuthal and radial flow components. Thus these analyses provide strong confirmation of the theoretical predictions, being able to explain not just the general features, but also the differences among storms. It is likely that the differences in the shape of the vertical profiles of wind in Fig. 2 is due to differences in the structure of the respective storms.

5.2. *Boundary Layer Stability Effects*

Stability is known to have a profound influence on the atmospheric boundary layer. Richardson number-based arguments show this effect will be smaller in the tropical cyclone boundary layer than elsewhere, but not negligible. Powell and Black (1990) demonstrate that it is indeed important, producing a variation in the observed SWF of 0.1, of similar magnitude to the dynamical variations discussed above, with lower values corresponding to stable conditions.

Little further work has been done on this factor, but it is clearly important to complete understanding and the ability to accurately predict the tropical cyclone boundary layer flow.

5.3. *Transients and Instabilities of the Boundary Layer*

The tropical cyclone boundary layer supports a number of instabilities and transient structures. There is some overlap between this section and section 7.3 which considers general instabilities leading to spiral band structures. Here, attention is restricted to phenomena that are clearly part of the boundary layer, chiefly rolls. Section 7.3 discusses fine-scale spiral bands that occur only partly within the boundary layer.

Boundary-layer rolls are very common in the atmospheric boundary layer (e.g., Etling and Brown, 1993), and the circulations of these rolls can produce highly organized surface winds perturbations. Wurman and Winslow (1998) presented the first Doppler radar evidence for their existence in tropical cyclones, indicating intense horizontal roll vortices with an average width of 600 m roughly aligned with the mean azimuthal wind in Hurricane Fran near landfall. The amplitude of variation of wind speed in these rolls was large: bands of 40–60 $\mathrm{m\,s^{-1}}$ flow alternated with 15–35 $\mathrm{m\,s^{-1}}$. Katsaros *et al.* (2002) examined synthetic-aperture radar images of Hurricanes Mitch and Floyd and also found periodic kilometre-scale variation. More recently, Morrison *et al.* (2005) describe features that are significantly less streaky in appearance, to the extent that it is not entirely clear that they are the same phenomenon. The different radar technology used may have contributed to the differences.

Lorsolo *et al.* (2008) analysed the observed finescale structure of the boundary layer wind field in two landfalling hurricanes from tower and Dopper radar measurements, and found numerous spatially coherent linear features in

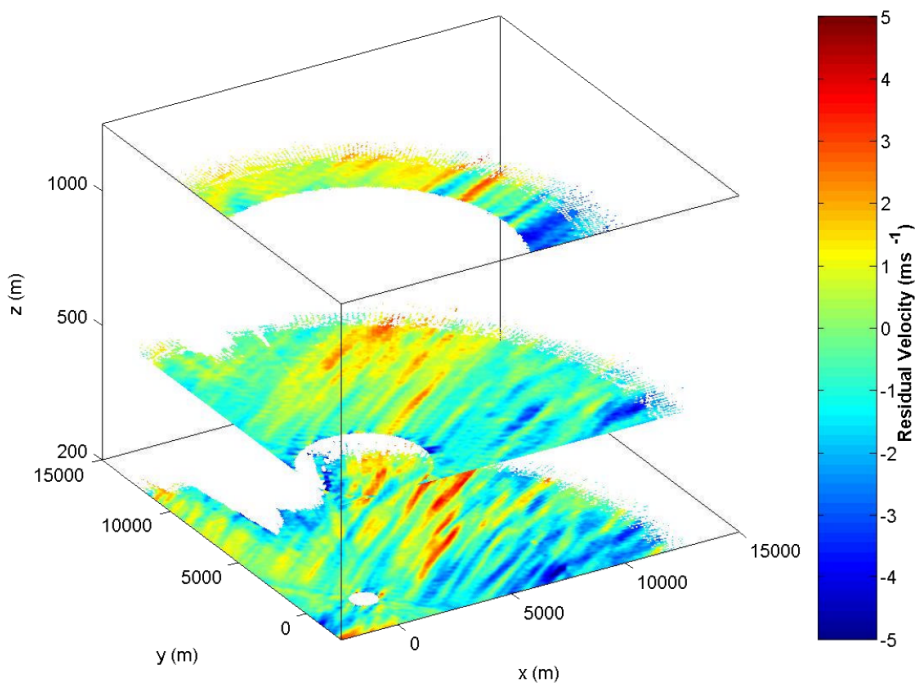

Figure 5. Horizontal cross-sections at 200, 500 and 1000 m altitude of Doppler radar residual velocities from a single radar volume in Hurricane Frances during landfall on 5 Sept. 2004. From Lorsolo *et al.* (2008).

the residual velocity field (Fig. 5). These features have an amplitude of up to $\pm 6\,\mathrm{m\,s^{-1}}$, are coherent through the depth of the boundary layer (500–1000 m), have a mean wavelength of ∼600 m, and are oriented on average 7° to the left of the surface flow, with a slight tendency for the orientation to rotate anticyclonically with increasing height. Radar- and anemometer-measured winds are in good agreement, demonstrating that the roll circulation extends to the surface, albeit with other scales of motion superimposed. However, they did not have sufficient data to determine whether these features did possess the full boundary layer roll circulation. Thus these features could contribute to observed damage streaks (e.g., Wakimoto and Black, 1994).

Theoretical analyses of roll development in tropical cyclones have been provided by Foster (2005) and Nolan (2005). Foster (2005) argues that the tropical cyclone boundary layer is an ideal environment for roll development. His argument extends the classical theory of roll development as an inflection-point instability of the frictionally-induced cross-isobar flow to the case of a tropical cyclone. Here, the cross-stream shear and hence instability are strong because the boundary layer is relatively shallow, and because the cross-stream component in analytical solutions is stronger than in classical Ekman-like solutions for straight flow (section 5.1.2). Nolan (2005) presents a stability analysis of a symmetric vortex, and finds both symmetric and asymmetric responses. The instabilities acquire some energy from the shear in the radial flow near the top of the boundary layer. In this regard they are similar to the rolls of Foster (2005). However, Nolan shows that the vertical shear of the azimuthal wind can also contribute energy to the instability, and that the relative importance of these mechanisms depends on both the inertial stability of the storm and the orientation of the mode.

6. Parametric Representation of Tropical Cyclones

Operationally, tropical cyclone are frequently defined by a few parameters, such as the intensity, RMW, and so forth. This supposes an ability to reconstruct the vortex based on those parameters. Such reconstructions are frequently used to force storm surge and wave models, or models of wind damage applied to an urban area, and are thus useful for applications ranging from operational forecasting and warning, to climatological risk assessment and engineering design. They also have a valuable role for initialising numerical models, both for idealised studies and for improving the initial vortex specification in numerical weather prediction models. Lastly, they may provide a framework within which to analyse observations.

A large number of such representations exist. Here, we will consider those of Holland (1980) and Willoughby *et al.* (2006). We omit one popular choice, the modified Rankine vortex, which was however discussed by Holland (1987) and Willoughby (1995).

The Holland (1980) profile model is an extension and improvement of earlier work by Schloemer (1954), in which the radial pressure profile is[6]

$$p(r) = p_c + \Delta p \exp(-(r_m/r)^b). \qquad (30)$$

Here, p_c is the central pressure, Δp is the pressure drop from the environment to the centre, r_m is the radius of maximum cyclostrophic winds, and b a shape parameter. Holland's original analysis assumed constant density with radius, but for lower tropospheric applications where the warm core is weak, it is better to take the virtual temperature T_v as constant with radius and allow ρ to vary through (8). The density at r_m is then $\rho_m = (p_c + \Delta p/e)/(R_d T_v)$ giving the maximum cyclostrophic wind v_{mc}, $v_{mc}^2 = e\Delta p/(b\rho_m)$ where e is the base of natural

[6]Noting that Holland uses $a = r_m^b$.

logarithms. The central pressure deficit is thus $\Delta p = p_c v_{mc}^2 e/(bR_d T_v - v_{mc}^2)$, whence the gradient wind equation (10) gives

$$v_{gr}(r) = -\frac{fr}{2} + \sqrt{\frac{v_m^2\,(r_m/r)^b \exp[1-(r_m/r)^b]}{1+\{\exp[1-(r_m/r)^b]-1\}\,v_m^2/(bR_dT_v)} + \left(\frac{fr}{2}\right)^2}, \tag{31}$$

a form in which the small difference between gradient and cyclostrophic balance near r_m is clear. In situations where a surface wind is required, boundary layer effects are usually crudely represented by reducing the gradient wind by an empirical factor of around 0.8, applying a cross-isobar angle of 20 to 30°, and adding on a wavenumber-1 asymmetry to represent the motion-induced asymmetry, although the use of a simplified dynamical boundary layer model would likely be an improvement.

The Holland profile has been by far the most extensively used parametric profile. Its popularity is probably due to a balance between its simplicity, with few physical parameters to choose, and its ability to give reasonably accurate representations of the majority of cyclone wind fields. Nevertheless, detailed comparison with observations reveals the following limitations: (i) the belt of strong winds near the RMW tends to be too wide, (ii) the wind decreases too rapidly with radius outside two or three times the RMW and (iii) the area of light winds inside the eye can be too large (Willoughby and Rahn, 2004). Other parametric profiles tend to share these limitations, particularly the first.

Recently, Willoughby *et al.* (2006) have presented a parametric profile which overcomes some of the limitations of other profiles, including that of Holland (1980). In particular, it allows a sharper maximum at the RMW, and allows the shape of the profile within and outside of the RMW to be independently adjusted. Unlike Holland's, which is written in terms of pressure and must be differentiated to find the equivalent gradient-wind, Willoughby *et al.*'s is written in terms of wind and must be integrated to find the pressure.

The Willoughby *et al.* (2006) wind profile may be written

$$v_1(r) = (v_{m1} + v_{m2})(r/r_m)^{n_1}, \quad \text{inside blending zone} \tag{32}$$

$$v_2(r) = v_{m1}\exp((r_m - r)/L_1) + v_{m2}\exp((r_m - r)/L_2), \quad \text{outside blending zone} \tag{33}$$

$$v(r) = (1-\alpha(r))v_1(r) + \alpha(r)v_2(r), \quad \text{within blending zone.} \tag{34}$$

The profile consists of the weighted mean of an eye profile v_1 with shape defined by n_1 ($n_1 < 2$), and an outer wind profile v_2 which is the sum of two exponentials of length scales L_1 and L_2, and amplitudes v_{m1} and v_{m2}. The maximum wind is $v_m = v_{m1} + v_{m2}$ at the RMW r_m. The weighting function $\alpha(r)$ is a 9th-order polynomial which increases monotonically from 0 to 1 across a blending zone of width $2L_b$ which contains r_m, with four continuous derivatives at each end of the blending zone. The location of the blending zone is determined by the requirement that the maximum wind occur at r_m, and found by solving $\partial v/\partial r = 0$ at r_m. Physically, the eye-profile v_1 can range through solid-body rotation ($n_1 = 1$) to something more U-shaped. The profile with only one exponential (i.e. $v_{m2} = 0$) is often adequate except for storms with a large radius of gales. It should be noted that these parameters are not independent; for example, more intense storms are usually more peaked (smaller exponential length scales), have more U-shaped wind profiles within the eye (larger n_1) and smaller RMW. The corresponding radial pressure profile can be obtained by radially integrating the gradient wind equation applied to (32), best done taking the T_v constant with radius as above. The profile

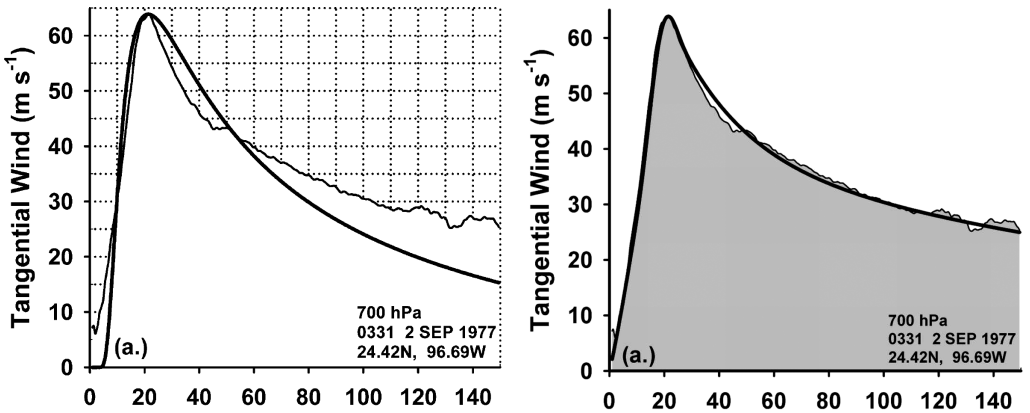

Figure 6. Observed azimuthal-mean azimuthal wind profile at 700 hPa in Hurricane Anita on 2 Sept. 1977, together with fits of equations (31) (left panel) and (32) (right panel) to the observations. From Willoughby and Rahn (2004) and Willoughby *et al.* (2006).

is not amenable to analytical integration and a numerical method is needed (Kepert, 2002c, appendix 4.A2).

The Willoughby *et al.* (2006) profile agrees better with aircraft observations than does Holland (1980), as shown for example in Fig. 6, but has so far received little use. A reason for this may be that fitting it to data involves dealing with a greater number of parameters, and that the fitting process can be poorly conditioned unless some of the parameters are held constant, as recommended by Willoughby *et al.* (2006).

Examination of aircraft data reveals that immediately outside of the RMW, the azimuthal-mean tangential wind decays relatively slowly, leading to a vorticity structure in which the very high values within the RMW are surrounded by a skirt of significant cyclonic vorticity (Mallen *et al.*, 2005). This skirt is absent in some parametric profiles, which instead have an annulus of anticyclonic relative vorticity some distance outside the RMW. While the differences in the wind field are small, the implications for vortex dynamics can be large, since (as will be seen) it is the radial vorticity structure that determines the dynamics of vortex Rossby waves and hence influences the response of the vortex to environmental vertical shear.

Freshwater flooding is a major cause of loss of life and property damage in landfalling tropical cyclones, so there is a need for parametric models of rainfall distribution as well as for wind. A simple model, R-CLIPER, described in Tuleya *et al.* (2007), is limited in that it generates an axisymmetric rain field. Recently, Lonfat *et al.* (2007) describe a rainfall model that includes representations of the spatial asymmetries caused by environmental shear as well as topographic rainfall enhancement.

7. Spiral Bands, Waves and Instabilities

Early radar observations revealed the ubiquitous presence of large-scale spiral bands of cloud and precipitation extending outwards from the eyewall (e.g., Maynard, 1945; Wexler, 1947). More recently, high-resolution radar measurements and careful analysis have shown the presence of abundant bands on much smaller scales as well (e.g., Gall *et al.*, 1998; Kusunoki and Mashiko, 2006). This section will discuss the structure, properties and dynamics of these various bands.

A substantial body of work has attempted to relate observed spiral bands to inertia-buoyancy waves. The connection has not been particularly successful, partly because of the observed

scale interactions between cumulus cells and the rain band, and partly because of the difficulty of matching the observed wavelength and propagation characteristics of the bands to the theory. This body of work will not be discussed here; instead, the reviews of Willoughby (1988, 1995) are recommended.

More recent work (Montgomery and Kallenbach, 1997; McWilliams *et al.*, 2003) has elucidated the properties of vortex Rossby waves (VRWs). These are similar to the planetary Rossby wave, except that it is the cyclone's radial vorticity gradient, rather than the planetary vorticity gradient, that provides the restoring influence. They are not identical, however, and the circular geometry leads to some significant differences. The relationship with vortex merger and the resulting vorticity filamentation will be explored, as will their role in cyclone intensification. Possibly the most spectacular manifestation of VRWs is the formation of eyewall mesovortices, which will be seen to have an important influence on cyclone structure, dynamics and thermodynamics. Vortex Rossby waves possess critical and turning radii and so are confined to relatively narrow radial bands.

Spiral rainbands are sometimes called "feeder bands", a term that implies that they help the development of the storm by providing a conduit for moisture to reach the eyewall. It will be seen that they may also transfer PV inwards. On the other hand, they involve the release of latent heat away from the eye, which is less efficient for intensification in balanced vortex models (Hack and Schubert, 1986). The question of the role of rainbands in storm energetics is important, but will be seen to be unresolved so far.

7.1. *Rainband Structure*

Rainbands are trailing spiral bands containing a mixture of stratiform and convective cloud and precipitation. Several observational studies have detailed the structure of individual bands (Barnes *et al.*, 1983; Powell, 1990a,b). There can be significant differences of detail between such case studies, and it is not clear as to the factors that determine these differences[7]. The crossing angle of the band axis is typically around 20°. Because bands spiral cyclonically inwards and the flow above the boundary layer is nearly circular, the cross-band relative flow is typically from the inside of the band outwards except in the lowest few kilometres. There the flow component perpendicular to the band is in the opposite direction, from the outside in. At these levels, the band forms a partial barrier to the cross-flow, with strong inwards flow on the outer side of the band and either weaker or zero inflow on the inner. Strong low-level convergence and upwards motion are associated with this barrier. The along-band and azimuthal flow components usually show a maximum on the outer side of the band axis, which is least qualitatively consistent with the greater radial advection of angular momentum there.

Convective cells, and their associated updrafts and downdrafts, are most common on the inward side of the band axis and at the upstream end of the band, near the low-level convergence maximum. The band-relative cross-flow leads to a stratiform anvil extending mainly towards the outer side of the band, with a smaller or absent anvil on the inner side. Similarly to squall-line convection, mesoscale subsidence of cool dry air beneath the anvil leads to a mass of low θ_e air above the boundary layer. This air forms part of the inflow into the band, where it promotes the development of convective downdrafts. The convective-scale vertical motions on the inner side of the band thus play an important vertical mixing role, bringing low θ_e midtropospheric air to the surface in cool dry downdrafts and transporting high θ_e air upwards. The low-level θ_e may be as much as 20 K lower on the inner side of the band than on the outer.

[7]Care is also needed in interpretation because while most studies utilise storm-centred cylindrical coordinate system, a few use a coordinate system aligned with the band axis.

That the rainband "consumes" low-level θ_e in this manner, thereby depriving the eyewall updraft of some fraction of energy, seems to be the typical but is not the only configuration. A rainband in Hurricane Gilbert showed no such decrease of θ_e on the inside of the band, and a strong radial gradient on the outer side which was too large to be due to surface fluxes alone. The inflow boundary layer that contained this strong gradient lay beneath a layer of strong outflow of high θ_e air, and the downward flux through the top of the boundary layer was, in conjunction with the surface fluxes, sufficient to explain the strong radial θ_e gradient. The outflow layer in this case also precluded the usual inflow of low θ_e subsiding air from beneath the stratiform anvil into the outer side of the band, necessary for the development of downdrafts and the resulting wakes on the inner side of the band (Barnes and Powell, 1995).

A wide rainband in an incipient tropical cyclone (Ryan *et al.*, 1992) had a similar but less organised structure. Principal differences were that the convergence was over ∼60 km and convection over ∼80 km widths, rather than the 5–10 km and 10–25 km respectively of the above studies. The convergence was from both sides of the band, and was *not* concentrated into a narrow band. This band produced just a weak cool pool from shallow downdrafts, rather than a strong cold wake from marked downdrafts.

7.2. *Vortex Rossby Waves*

The similarity between planetary Rossby waves and tropical cyclone spiral bands was first noted by MacDonald (1968), with a major interest being the upgradient flux of angular momentum due to trailing waves. Montgomery and Kallenbach (1997) derived the dispersion relation for the nondivergent barotropic inviscid case:

$$\omega = n\overline{\Omega}_0 + \frac{n}{r}\frac{\overline{\zeta}_0'}{k^2 + n^2/r^2} \tag{35}$$

where the instantaneous radial wave number is

$$k(t) = k_0 - nt\overline{\Omega}_0' \tag{36}$$

and symbols are defined in Table 2. Radial and azimuthal phase and group velocities derived from (35) are given in Montgomery and Kallenbach (1997). Comparing (35) to the dispersion relation for nondivergent Rossby waves on a β-plane reveals strong similarities, justifying their nomenclature of "vortex Rossby wave". An important difference in cyclones is that the radial wavenumber k varies with time and position, because of the radial shear in the vortex basic state flow. Equation (36) thereby implies that the radial phase speed of a wave will approach 0 as time increases. Möller and Montgomery (2000, Eq. (3.3)) extend (35) to the case of waves with vertical structure.

Consider a northern hemisphere tropical cyclone with $\overline{\Omega}_0 > 0, \overline{\zeta}_0 > 0, \overline{\Omega}_0' < 0$ and $\overline{\zeta}_0' < 0$. Segments of trailing spirals can be described by $k > 0$ and $n > 0$. Then the azimuthal phase velocity ω/k is less than the flow speed $r\Omega_0$ at that radius and the waves retrogress, similar to planetary Rossby waves. The radial group velocity is initially outwards, but decreases to 0 with time due to the increase in radial wave number. Thus the increase in $|k|$ with time causes the waves to possess a stagnation radius, so they are confined to the vortex vicinity and cannot radiate to infinity. The growth of k in time also implies that inwards-propagating, leading spirals will eventually become outwards-propagating and trailing, consistent with observations.

Studies of the interaction of constant vorticity patches in, for example, nondivergent barotropic "contour dynamics" models, frequently show the formation of trailing filaments of vorticity as in, for example, Ritchie and Holland (1993) and Guinn and Schubert (1993), similar to the filaments that arise in the VRW theory. Differences between contour dynamics models and the VRW analysis above is that the vorticity filaments in the former are simply advected, as there is no continuous radial vorticity gradient in such models to provide

the Rossby wave propagation mechanism. The contour dynamics models, on the other hand, demonstrate several mechanisms for the formation of the filaments, including the stretching out and shearing of one vortex patch by another and the inherent instability of sufficiently elliptical vortex patches (Melander *et al.*, 1987; Ritchie and Holland, 1993; Velasco Fuentes, 2004).

The filaments of vorticity around the main vortex, in either class of model, imply wind perturbations. Aircraft observations (Samsury and Zipser, 1995) show that most secondary wind maxima in tropical cyclones are co-located with reflectivity maxima, suggesting that vorticity bands are rainbands. In contrast, most rainbands lack a detectable wind maximum, so the converse may not be true.

Numerical simulations of sufficient resolution show spiral band features in the inner core with a high correlation between precipitation, clouds and PV in the bands, implying that these bands are coupled to VRWs (Chen and Yau, 2001; Wang, 2002a,b). Empirical normal mode analysis showed that 70–80% of the wave activity of the larger-scale asymmetries ($n = 1, 2$) could be attributed to VRWs, with gravity waves playing a much smaller role (Chen *et al.*, 2003).

Observations also provide strong support for the connection between these bands and VRWs, with Reasor *et al.* (2000) demonstrating a strong correlation between $n = 2$ bands of Doppler-derived vorticity and reflectivity in Hurricane Olivia. Corbosiero *et al.* (2006) analysed radar data in Hurricane Elena (1985). In the six hours leading up to peak intensity, the eye became elliptical in shape, with the major axis rotating at about half the wind angular velocity. The elliptical shape was due to a pair of eyewall mesovortices (section 7.4). Periodically, $n = 2$ components of reflectivity broke off the outside of the eye and propagated azimuthally at 68% of the mean flow (i.e. retrograde motion) and outwards at about $5.2\,\mathrm{m\,s^{-1}}$. Both motion components were shown to be consistent with the phase and group velocities implied by (35). Figure 7 shows the sequence of radar reflectivity corresponding to one of these instances.

While VRW theory is quite consistent with both observations and simulations in full-physics models, two significant limitations are apparent. Firstly, the agreement at wavenumbers $n = 3$ and higher is less satisfactory, possibly because on smaller scales the dynamics is more influenced by the coupling to convection and also because of the inherent noisiness of nonlinear fluid dynamics at such scales. The smaller-scale bands, and their possible mechanisms, are discussed further below. The second limitation is that the VRWs have a stagnation radius that is typically about 3 times the RMW, and also that the radial gradient of PV becomes weak at around this radius (Montgomery and Kallenbach, 1997; Wang, 2002a,b). Hence the theory of Montgomery and Kallenbach (1997) is not applicable outside of the vortex core. McWilliams *et al.* (2003) present a more comprehensive theory that includes this case, and show that the waves become nondispersive with only azimuthal propagation (see their appendix A.2), consistent with the results of the contour dynamics calculations cited above.

7.3. *Finer Scale Bands*

Aside from the large-scale spiral bands, Fig. 8 shows evidence for numerous bands on the $\sim$10 km scale from radar observations and models (Gall *et al.*, 1998; Kusunoki and Mashiko, 2006). Unlike the larger-scale bands, these bands are simply advected by the mean flow, displaying even less propagation than VRW theory would imply. Similar fine-scale bands have been found in high-resolution numerical simulations by Yau *et al.* (2004) and Romine and Wilhelmson (2006). The modelled bands have a high (but not complete) correlation between PV, w, precipitation and low-level wind maxima, suggesting a significant role for moist dynamics. Cross-sections of the bands from the above observational and

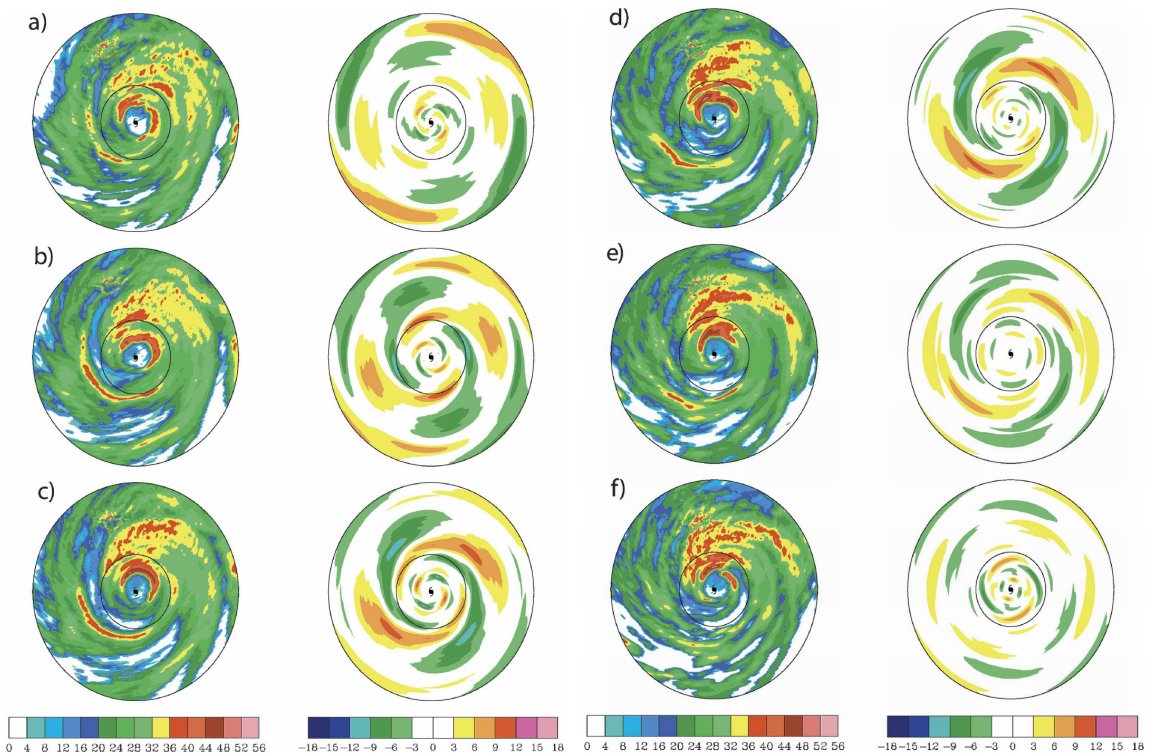

Figure 7. Radar reflectivity (left) and $n = 2$ asymmetry (right) of Elena at (a) 1600, (b) 1620, (c) 1640, (d) 1700, (e) 1720 and (f) 1740 UTC 1 Sep. The circles mark the 50- and 150-km radii. From Corbosiero *et al.* (2006).

modelling studies are compared in Fig. 8. Instability of the strong low-level shear in the radial inflow, somewhat similar to that that leads to the formation of boundary layer rolls but modified by moisture and stability variations, may also play an important role (Nolan, 2005; Foster, 2005; Romine and Wilhelmson, 2006). To date, comprehensive analyses of wave dynamics exist only for larger-scale waves, and analyses of flow stability exist only for relatively idealised situations, so the relative importance of radiating PV waves versus flow instability in the dynamics of these finer-scale bands is unclear.

7.4. *Eyewall Mesovortices*

The existence of small vortices, of ∼10 km scale, abutting the inner edge of the eyewall, has been known for some time and linked to the occasional occurrence of a markedly polygonal structure of the inner edge of the eyewall on radar reflectivity images (e.g., Muramatsu, 1986). These polygonal eyewalls typically had between 3 and 6 sides, and rotated somewhat more slowly than the azimuthal flow. Aircraft observations (Marks and Black, 1990; Black and Marks, 1991) showed that in extreme cases, an eyewall mesovortex (EMV) could possess local wind and pressure perturbations of magnitude approaching that of the primary vortex core. A spectacular recent example was the six EMVs observed in Hurricane Isabel, shown in Fig. 9 (Kossin and Schubert, 2005).

Kossin and Eastin (2001) used aircraft data to show that the wind and thermodynamic structure of strong tropical cyclones evolve between two distinct regimes. In regime I, the radial profile of wind across the eye is U-shaped, with maximum angular velocity within

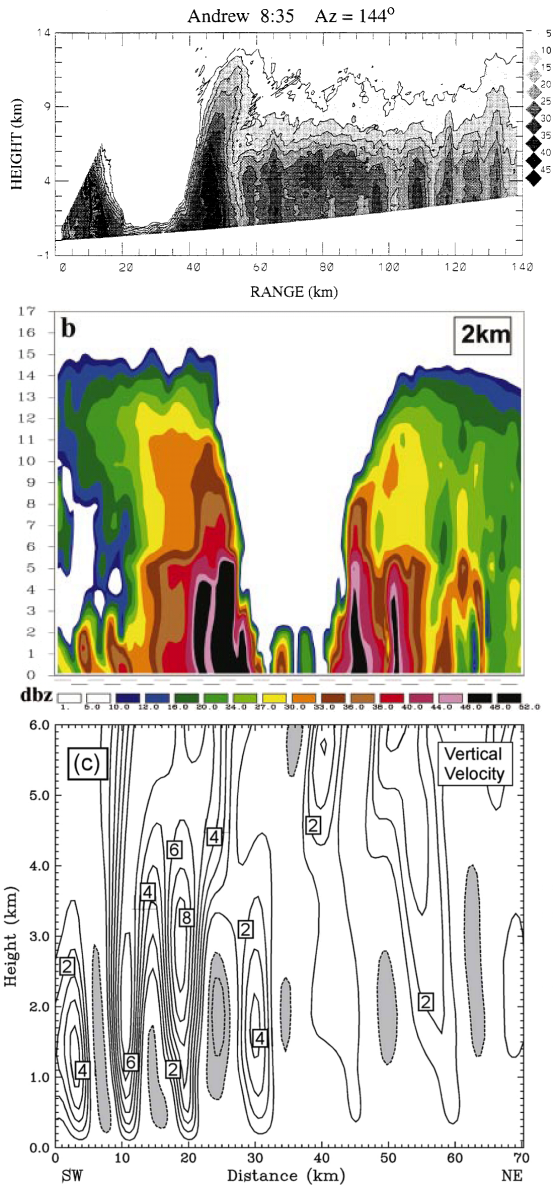

Figure 8. Radius-height sections of fine-scale bands in tropical cyclones. Top: Radar reflectivity observations in Hurricane Andrew, from Gall *et al.* (1998). Middle: Simulated reflectivity in a high-resolution simulation of Hurricane Andrew, from Yau *et al.* (2004). Bottom: Vertical velocity in a high-resolution simulation of Hurricane Opal, from Romine and Wilhelmson (2006).

the eyewall, and an annular ring of vorticity just inside of the RMW. The eye is typically warm and dry, with elevated values of θ_e in the eyewall and lower values within the eye.

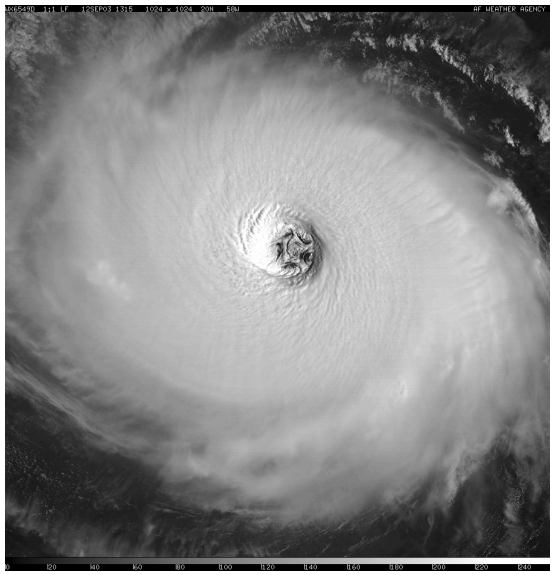

Figure 9. Defense Meteorological Satellite Program visible image of Hurricane Isabel at 1315 UTC 12 Sep 2003. The six mesovortices — one at the centre and five surrounding it — cause the starfish pattern in the eye. From Kossin and Schubert (2005).

Regime II, in contrast, is characterised by a V-shaped wind structure within the eye, with vorticity and angular velocity maxima near the centre of the eye. The air in the eye is relatively moist, with a θ_e maximum near the vortex centre. The transition from regime II to I occurs relatively slowly, as a consequence of the secondary circulation within the eye (section 3). In contrast, the reverse transition can be very rapid, and may occur in less than an hour. An example of the changes in the dynamical and thermodynamic variables during this transition is shown in Fig. 10. The simultaneous change in kinematic and thermodynamic variables suggests the sudden onset of intense horizontal mixing between the eyewall and the eye. This mixing appears to be caused by the onset of eyewall mesovortices (EMVs), consistent with the barotropic instability of regime I. Kossin and Schubert (2003) discuss how this mixing is distinct from a horizontal diffusion process.

This barotropic instability is similar to that in other strongly sheared flows. The regime I hurricane is approximately a hollow tower of

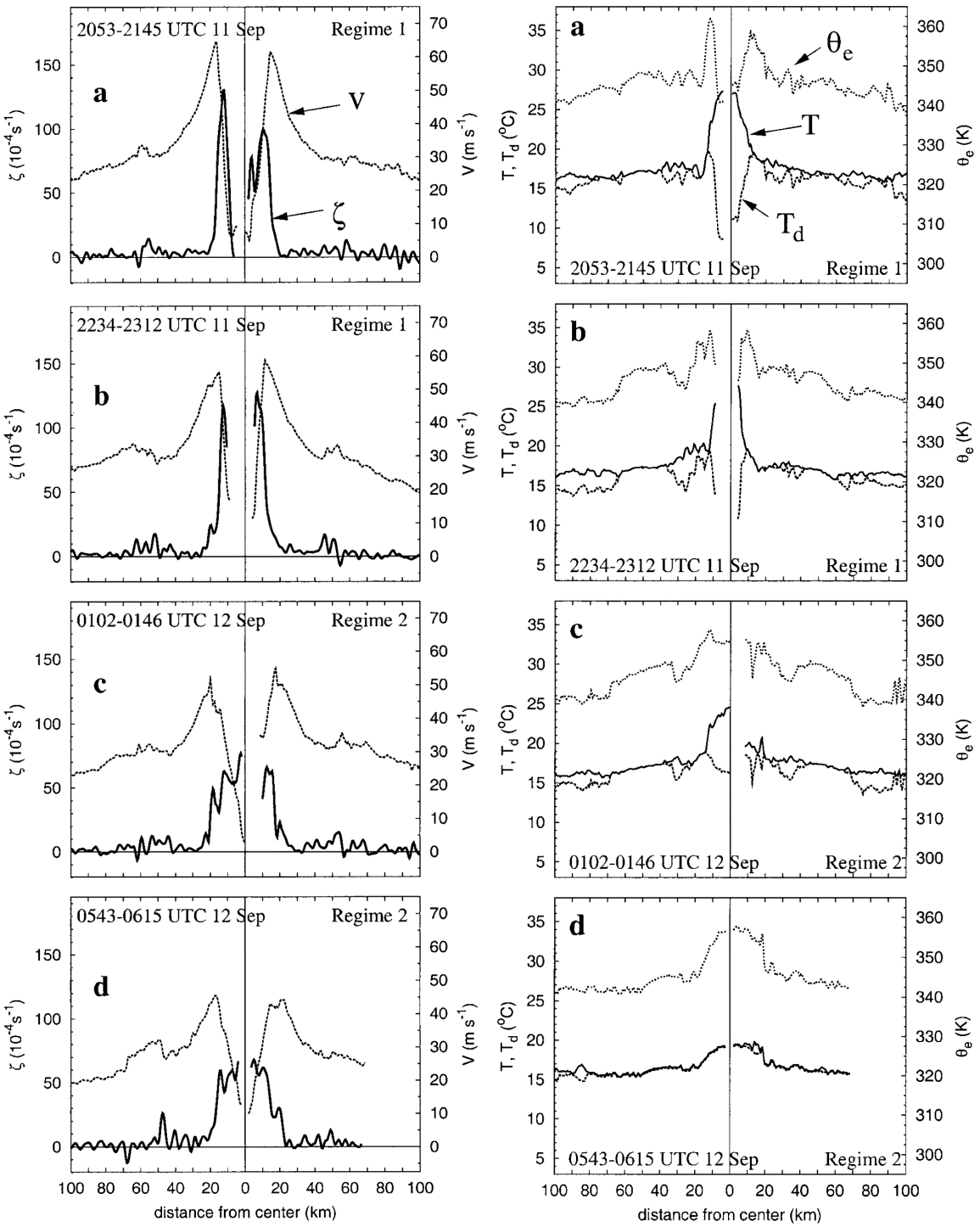

Figure 10. Time-sequence of observed flight-level dynamical (left) and thermodynamic (right) parameters at 850 hPa in Hurricane Diana (1984), showing the transition from Regime I to II. During the transition, v goes from a U-shaped to a V-shaped profile, ζ and θ_e from hollow ring to monopole structures, and the air in the eye becomes saturated. From Kossin and Eastin (2001).

vorticity (located just inside of the RMW), with less vortical flow inside and out. Vortex Rossby waves can propagate on both surfaces of the tower: on the inner face, the propagation is with (i.e. faster than) the flow, while on the outer face, it is against (slower). It is thus possible that the inner and outer waves can phase lock and mutually amplify, leading to exponential growth of the waves. This process was modelled in an unforced barotropic model by Schubert *et al.* (1999), who showed that the vortex ring could break down into several mesovortices, which subsequently merged to form a vortex monopole. Thus the wind profile went from U-shaped to V-shaped; precisely the change noted in aircraft data by Kossin and Eastin (2001). A range of final vortex structures is possible, depending on the size, width and strength of the initial vortex ring. Kossin and Schubert (2001) explore the part of the parameter space relevant to tropical cyclones. The typical response is for the vortex ring to break into a relatively large number of mesoscale vortices, which subsequently merge. These mergers may proceed to give a single discrete vortex monopole, or to a quasi-stable "vortex crystal", an asymmetric lattice of mesovortices rotating as a solid body. The flow due to such a structure consists of near-straight line segments, making up a persistent polygonal shape. Such lattices can also undergo internal rearrangements — e.g. from a pentagon with a central mesovortex to a hexagon, and back again. The former of these structures is strikingly similar to the well-known instance of mesovortices in Hurricane Isabel (Fig. 9).

Detailed observations of eyewall vorticity maxima have been presented in Hurricane Hugo by Marks *et al.* (2008) and in Hurricane Isabel by Aberson *et al.* (2006). The vortex in Hugo had a diameter of ∼1 km at 450 m altitude with wind and pressure perturbations of $23\,\mathrm{m\,s^{-1}}$ and 12.5 hPa respectively, a peak updraft of $21\,\mathrm{m\,s^{-1}}$ and a peak cyclonic vorticity of $1.25 \times 10^{-1}\,\mathrm{s^{-1}}$. Hugo's eye also contained a larger-scale cyclonic circulation, about 15 km across, that orbitted the eye with a period of ∼19 min, or roughly the angular velocity of the axisymmetric mean vortex, consistent with the wavenumber-1 asymmetry investigated by Nolan and Montgomery (2000) and Nolan *et al.* (2001). The vortex in Isabel produced a dropsonde horizontal wind observation of $107\,\mathrm{m\,s^{-1}}$ and an updraft of $25\,\mathrm{m\,s^{-1}}$ when the vortex mean low-level winds were around 70 to $80\,\mathrm{m\,s^{-1}}$. Radar reflectivity data suggest a horizontal scale similar to that in Hugo. If such wind anomalies extend to the ground, they likely represent a mechanism for increased damage potential that has not been widely appreciated.

These dramatic rearrangements of vorticity are accompanied (in the model) by equally spectacular pressure changes. In the change from the U-shaped (vorticity hollow tower) to the V-shaped (vortex monopole) structures, the winds inside the eye accelerate dramatically, while the maximum wind decreases. Integrating the gradient wind equation inwards, the net effect is that the central pressure falls substantially, even while the intensity as measured by the strongest winds decreases. Similar vortices have been produced in the laboratory: Montgomery *et al.* (2002) describe a water-flow apparatus which produces a curved shear layer, with primary and secondary circulations and aspect ratio similar to a hurricane. Two quasi-steady vortices, together with intermittent secondary vortices, form from shear instability of the curvilinear shear layer on the inner side of the "eyewall". The peak tangential velocity occurred within the mesovortices, and was ∼50% stronger than that of the parent vortex.

An eye structure intermediate between the Kossin and Eastin (2001) regimes and possessed by tropical cyclones with an unusually high degree of axisymmetry was identified by Knaff *et al.* (2003, 2008) and named "annular hurricanes". They are also known as "truck tyres" from their appearance on IR satellite imagery. These storms apparently form from the asymmetric mixing of eye and eyewall, possibly by mesovortices, but the mixing does not proceed all the way to the monopole

structure of regime II. Annular hurricanes form within certain specific and relatively rare environmental conditions, including weak westward and equatorward environmental shear and favourable thermodynamics, as measured by the PI. In addition to the large, symmetric eye, they are also unusually symmetric outside the eye, with little evidence of outer rainbands. Significantly for forecasting, they maintain intensity longer and weaken more slowly than other tropical cyclones, and are thus a significant source of intensity forecast error.

Much of the interest in EMVs has been in highly symmetric storms with a clear eye in the cirrus overcast, since this facilitates their identification from satellite imagery. However, numerical simulations (Braun *et al.*, 2006; Halverson *et al.*, 2006) have shown that EMVs also exist in sheared storms, where the storm axis is tilted. A tilted axis has enhanced low-level convergence and ascent on the downtilt side, leading to increased rainfall downtilt-left in the northern hemisphere (section 8). The opposite applies uptilt. These papers showed that EMV-like features may orbit the tilted eyewall, with their updraft and vorticity intensifying as they move into the favourable downtilt area, and weakening as they leave it. Cyclonic advection of the enhanced EMV convection led to the coldest cloud tops being on the upshear side of the storm in Hurricane Erin.

7.5. *The Effect of Spiral Bands on Storm Intensity*

Spiral bands may act to reduce intensity, since they consume some of the energy-rich boundary layer inflow and replace it with cool dry downdrafts (section 7.1). However, this energy is replenished by surface fluxes (section 5.1) so this effect may not be large. The heat released in these bands contributes little to storm intensity, since the efficiency of heat release away from the inner core is less (Hack and Schubert, 1986).

On the other hand, spiral cloud bands may form a "buffer" that helps to protect the storm from the effects of environmental shear — there is some observational evidence that large storms are better able to resist shear than small.

Samsury and Zipser (1995) have shown that at least some spiral bands accompany along-band wind maxima, and hence vorticity bands. Their results may well be an underestimate of the frequency with which rainbands contain elevated vorticity, since they had observations at only one level and reported only the incidence of local wind maxima, which would be present for only sufficiently strong vorticity maxima. To the extent that rainbands are vorticity bands, they are vorticity bands that are tilted downshear in a stable sheared flow and will support an upgradient, or inwards, flux of vorticity (Carr and Williams, 1989; Montgomery and Kallenbach, 1997; Nolan and Farrell, 1999; Möller and Montgomery, 1999, 2000; May and Holland, 1999; Chen *et al.*, 2003). Such bands will tend to intensify the storm. On the other hand, Nolan and Grasso (2003) and Nolan *et al.* (2007) have argued that the adjustment process by which the bands form will tend to weaken the storm, and that the azimuthal-mean effect of the heating may be stronger than the vorticity flux.

8. Environmental Influences

Real tropical cyclones are embedded in an environment that includes the surrounding atmosphere, ocean and land, and which has a profound effect on the formation, development, maturity and decay of the storm. In this section, we will focus on the atmospheric part of the environment, with ocean effects in Chapter 3. Important topics include the effects of vertical shear on storm structure and intensity change, and the effects of upper troughs.

Shear is long recognised as an important factor, starting with the original ventilation concept; that is, the tendency for the sheared environment to move the upper level warm core away from the surface circulation (Simpson and Riehl, 1958). Observational and modelling studies agree that there is a shear threshold

for weakening of a mature storm, that weakening may not occur immediately with the onset of shear, and that the detailed response depends on storm intensity and structure. Wind shear causes a substantial asymmetry in the storm's precipitation field. Whether this translates into an asymmetry in the precipitation swath depends on the shear-relative motion, with along-shear motion resulting in an asymmetric precipitation swath. The environmental moisture around a storm can also influence its response to shear.

Trough interactions are an important effect that is difficult to diagnose, with opinion divided as to their role overall and in individual cases. Dynamically, most studies are founded on the idea that eddy fluxes of angular momentum may most easily influence the storm core in the upper levels due to the low inertial stability there (section 3). However, upper troughs often coincide with an increase in the vertical shear. Evidence seems to be that both intensifying and weakening influences are possible, but the problem of differentiating "good" from "bad" troughs is far from solved. They also form an essential component of extra-tropical transition, discussed in Chapter 5.

When a number of significant environmental influences exist, determining the net effect of the combination can be complex. For instance, the weakening effect of strong wind shear may be reduced if the storm is over a region of high ocean heat content, or increased if the environmental air is unusually dry.

8.1. *Dry Dynamics*

Imposing vertical shear on a vortex will cause it to tilt in the direction of the shear. The resulting evolution can be qualitatively understood by considering a two-level system, in which the vortex is located at different positions in the two levels. The PV inversion principal (section 2.1) shows that the upper level of the vortex will project downwards and generate a cyclonic flow displaced from the lower vortex, while the lower vortex will similarly generate an upper-level circulation. These induced circulations will cause the upper and lower parts of the vortex to orbit each other; that is, the tilted vortex axis will precess with time (Jones, 1995). The rate of precession depends on the strength of the flow induced by the displaced PV fields at the two levels. It will therefore be stronger for a larger or more intense system and for lower static stability, since these changes both act to increase the penetration depth and strength of the induced flow (Jones, 1995; Smith *et al.*, 2000). If the shear is sufficiently strong, then the upper and lower vortices will separate. The threshold for this separation will depend on the strength of the interaction. In these dry simulations, the precession of the tilt axis continues until the vortex is tilted up-shear, whereupon the shear acts to temporarily reduce the tilt. However, following further precession, the tilt is again downshear and continues to increase.

For the flow in a tilted vortex to remain balanced, a warm anomaly must develop on the up-tilt side, and a cold anomaly down-tilt, so that (through hydrostatic balance) the pressure centre can have a similar tilt to the wind centre. Thus the isentropes are perturbed upwards on the down-tilt side, and downwards uptilt. As the flow follows these isentropes, maximum ascent occurs to the right of the tilt vector, with maximum descent to the left in the northern hemisphere. The strength of the vertical motion asymmetry and the potential temperature anomalies increase with the vortex tilt, until the vortex begins to weaken (Jones, 1995).

Vortex Rossby wave dynamics provide an alternative view of the evolution of the vortex tilt (Reasor and Montgomery, 2001; Schecter *et al.*, 2002). Here, the tilted vortex is decomposed into the sum of a vertical axisymmetric vortex, and a baroclinic perturbation with azimuthal wavenumber one and vertical structure of the first internal mode. That is, it consists of a cyclonic perturbation underlying an anticyclone on one side of the storm, with the opposite on the other side. Adding this

perturbation to the axisymmetric mean vortex gives a vortex with a tilted axis. The evolution of the sum can then be understood in terms of the VRW dynamics of the perturbation. These calculations assumed quasigeostrophic dynamics and so strictly apply only to weak tropical cyclones.

The response falls into one of two categories, depending on L_R (Reasor and Montgomery, 2001; Reasor *et al.*, 2004). For L_R larger than the horizontal scale of the vortex, the tilt mode projects onto an azimuthal wavenumber one quasi mode which rotates cyclonically with time and decays very slowly. The decay is essentially negligible on meteorologically relevant time-scales. This case is similar to the solutions of Jones (1995, 2000b) except that the vortex tilt decays slowly instead of growing indefinitely. At smaller L_R, the initial perturbations project onto a continuous spectrum of VRWs whose integrated perturbation energy decays algebraically to zero. This effect can be regarded as either due to constructive interference, or to the spiral wind-up of the waves. The original calculations used a quasigeostrophic model (Reasor and Montgomery, 2001), while later calculations for finite Ro (Reasor *et al.*, 2004) demonstrated a stronger resistance to tilt in this case, and showed that a vortex in shear arrives at an equilibrium with the vortex tilted to the left of the shear vector (in the northern hemisphere). The degree of tilt is greater in the outer vortex than in the core.

A distinct, but complementary view of the small L_R case is given by Schecter *et al.* (2002) and Schecter and Montgomery (2004), who show that the tilt mode decays exponentially with time due to resonant damping with a critical layer. The baroclinic mode propagates cyclonically, and so there exists a critical radius r^* at which the cyclone's azimuthal velocity matches the phase speed of the mode, and is thus the radius where the mean flow and the wave most readily interact. This interaction damps the wave, with concomitant decay of the vortex tilt, provided that the radial gradient of potential vorticity at r^* is negative. The decay is initially exponential, with rate proportional to the PV gradient at r^*. Hence for a zero gradient, the wave is neutral, while for a reversed (i.e. positive) gradient, the wave will grow and the vortex tilt will increase with time. The rate is higher for strong static stability and also depends on the internal Rossby radius of deformation L_R. The details of this latter dependence are sensitive to the structure of the axisymmetric vortex, and Schecter *et al.* (2002) present examples showing that the decay rate may either increase or decrease with increasing L_R.

The most important consequence of Schecter *et al.* (2002)'s results is that a tilted vortex will not align unless the radial gradient of PV at the critical radius is negative. For a zero gradient, the relevant modes are undamped and the vortex will not align. This situation may occur either in the limit of infinite L_R in any vortex since then $r^* \to \infty$, or in "compact" vortices in which the PV is entirely bounded by some radius. Furthermore, in vortices where the radial PV gradient is positive at r^*, the tilt mode will grow and the vortex is unstable to small tilts. Reasor *et al.* (2004) shows that many of the vortices in the simulations of Jones (1995, 2000b) possess this latter characteristic, and thus explains why many of her simulations show a general tendency for the vortex tilt to increase with time. The growth of tilt with time is therefore not a universal characteristic. Aircraft data show that the radial vorticity gradient in the lower to mid troposphere is generally negative to 3 times the RMW, a range which would normally include the critical radius r^*, and therefore real tropical cyclones are inherently stable to shear-induced tilt (Mallen *et al.*, 2005).

For initially baroclinic dry vortices, the situation is more complex. Simulations by Jones (2000b) show that the low- and mid-level centres orbit each other, while the upper level centre is usually advected away, and may shed vorticity filaments followed by axisymmetrization (e.g., Möller and Montgomery, 2000). These vortices

had the same radial structure as her studies with initially barotropic vortices, so the growth of tilt is consistent with the above VRW-based analysis. Frank and Ritchie (1999) presented a calculation in which the surface-500 hPa tilt grows indefinitely, but the upper-level centre has relatively less movement. Their initial vortex was broader and weaker than that of Jones (1995), but its stability to tilt is not known.

In this section, we have seen two distinct but related groups of theory describing the evolution of a vortex in vertical sheared environment. First we considered the mutual interaction of horizontally displaced upper and lower tropospheric masses, where the interaction proceeds via the vertical projection of the lower mass into the upper troposphere and vice versa and leads to a mutual rotation about each other, and hence a precession of the tilt axis. This analysis also explains a marked wavenumber one asymmetry in the vertical motion in the storm, with the maximum updraft on the downtilt side. The second body of theory decomposes the tilted vortex into a vertical axisymmetric vortex and a first internal mode, azimuthal wavenumber one perturbation, and describes the evolution of the tilt through the vortex Rossby wave dynamics applied to the perturbation. The response falls into two regimes: the quasimode with cyclonic progression accompanied by slow decay, and the spiral wind-up or resonant damping mode where the perturbation decays rapidly and the vortex thereby strongly resists the tilting effect of the environmental shear. The latter theory importantly identifies stability criteria that decide whether the vortex is inherently stable or easily sheared apart, with many of the vortices used for calculations with the first theory falling into the unstable category. Aircraft measurements show that most real tropical cyclones have a structure that is stable to tilt. However, the basic mechanism for precession of the tilt axis in slowly-decaying tilts in the second body of theory is essentially that for precession in the first. Moreover, the PV-interaction theory predicts a strong asymmetry in vertical motion that is highly consistent with observations of rainfall and cloudiness in tropical cyclones, and is therefore important to understanding and predicting this aspect of real cyclones. A further limitation of the VRW-based theory is that it has so far considered only barotropic vortices, and while it has been most fruitful for understanding the dynamics, this assumption may omit some potentially important aspects of the problem.

8.2. *The Influence of Moisture*

Idealised "full-physics" simulations of tropical cyclones in sheared environments have been presented by (for example) Wang and Holland (1996), Frank and Ritchie (1999, 2001), Peng *et al.* (1999), Kimball and Evans (2002), Wong and Chan (2004), and Ritchie and Frank (2007). The evolution of the tilt in all of these simulations is in stark contrast to the dry simulations of Jones (1995, 2000a,b) and Frank and Ritchie (1999), in that precession of the axis does not occur and a near-equilibrium of downshear-left tilt develops, except when the shear is sufficient to destroy the storm. The natural conclusion drawn from these results was that the secondary circulation produced by the diabatic heating acts to couple the upper- and lower-level centres and resist the tilting effects of shear. A more complete explanation was provided by Schecter and Montgomery (2007), who showed that clouds in the core of a monotonic vortex can cause or accelerate the decay of discrete VRWs, thereby increasing the resilience of the vortex to tilt (section 8.1). Another factor may have been that the diabatic processes cause the initial vortex to evolve towards a structure that is stable to tilt. Unfortunately, of the full-physics simulations listed above, only Wang and Holland (1996) provide sufficient information to determine the tilt-resilience of their vortex. Their initial vortices have monotonic radial PV gradients and are therefore tilt-resilient, except in the upper troposphere, where an upper anticyclone leads to a reversed gradient at about 300 km radius (their Fig. 1).

Moist simulations that consider a range of wind shears show that the effect of shear on intensity is larger for stronger shear, with a threshold of about 8–10 $m\,s^{-1}$ of shear for weakening to occur. There is often a time lag between the onset of shear and the onset of weakening, of from a few hours (very strong shear) to over 36 hours for 5 $m\,s^{-1}$ shear (Frank and Ritchie, 2001; Wong and Chan, 2004). Frank and Ritchie (2001) show that the storm weakens from the top down, and identify the following sequence of events: (i) the development of strong inner core asymmetries, (ii) the asymmetries in the upper core (where the storm circulation is relatively weak) become strong enough to mix heat and PV outwards, allowing the shear to ventilate the eye; (iii) the loss of the upper warm core causes the surface pressure to rise, weakening the storm; and (iv) downshear advection of the weakened upper levels causes downshear tilt of the storm. The top-down weakening ends when the ventilated layer can descend no further, due to the greater strength and inertial stability of the vortex at lower levels. Wong and Chan (2004) found that the sensitivity of the cyclone to shear depended upon the size of the storm, with smaller storms being less resistant.

Environmental shear causes marked asymmetries in vertical motion, cloudiness and rainfall in these moist simulations. The initial cause of these asymmetries is as in the dry simulations discussed above, but as the storm develops further, latent heat release destroys the cold downshear anomaly and the maximum updraft moves to the downshear-left quadrant, together with the maximum cloud water. The rainfall maximum occurs slightly downstream on the left of the shear (Fig. 11), due to advection of the precipitation as it falls (Wang and Holland, 1996; Frank and Ritchie, 1999, 2001; Wong and Chan, 2004). The difference between simulations on f- and β-planes seems to be largely that the β-gyres (see Chapter 4) are strongest at the surface and hence induce a few $m\,s^{-1}$ of equatorwards and eastwards shear over the storm core (Peng *et al.*, 1999; Ritchie and Frank, 2007). Thus the effective total shear is less for easterly environmental shear than for westerly, as the former is partly cancelled by the β-gyre-induced shear (Peng *et al.*, 1999; Ritchie and Frank, 2007).

The effect of these asymmetries on the rainfall swath depends on the relative directions of the shear and the storm motion. Where the shear is along-track, the rainfall occurs predominantly on the left of track. Conversely, for cross-track shear, this left-of-shear rain is distributed approximately symmetrically about the track (Rogers *et al.*, 2003).

8.3. *Observations of Shear and Intensity Change*

Several studies have examined the intensity change in tropical cyclones as a function of environmental shear. Statistical intensity forecast schemes (DeMaria and Kaplan, 1994, 1999; DeMaria *et al.*, 2005) have universally included environmental vertical shear is a statistically significant predictor, with the threshold between weakening and strengthening lying at about 10 $m\,s^{-1}$ of 850–200 hPa shear. Gallina and Velden (2002) found a strong linear correlation between shear and intensity change, with the transition between strengthening and weakening occurring at a shear of 7–8 $m\,s^{-1}$ in the North Atlantic, and 9–10 $m\,s^{-1}$ in the North West Pacific. They also noted a time lag between the onset of shear, and weakening. Paterson *et al.* (2005) similarly found that shear values above about 10 $m\,s^{-1}$ favoured weakening, and above 12 $m\,s^{-1}$ rapid weakening, in the Australian region, with a time lag of 12 to 36 hr between the onsets of shear and weakening. While this study found that weak shear (2–4 $m\,s^{-1}$) generally led to rapid intensification, a small group of storms failed to intensify even when the shear was very weak.

The Saharan Air Layer (SAL) is a layer of dry, dusty air between about 850 and 500 hPa, overlying a marked temperature inversion, with an easterly jet at about 700 hPa. When this feature engulfs a hurricane, the ventilation due

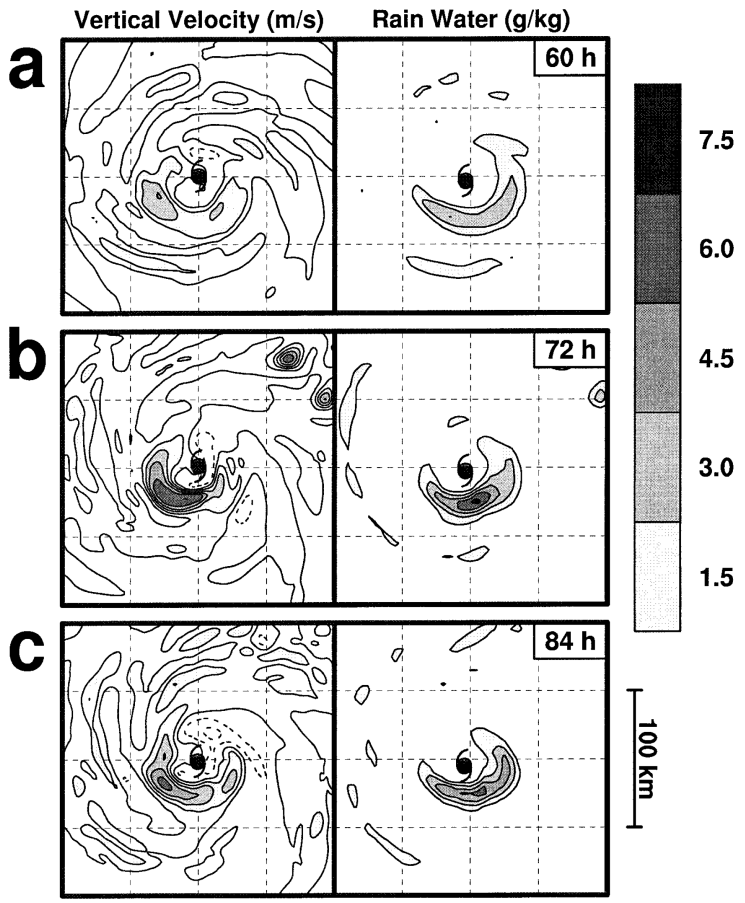

Figure 11. Evolution of vertical velocity ($\mathrm{m\,s^{-1}}$) and rainwater ($\mathrm{g\,kg^{-1}}$) at 700 hPa for an idealised simulation of a tropical cyclone in $5\,\mathrm{m\,s^{-1}}$ easterly shear on an f-plane. Domain size is 200 km square, dashed contours show negative values. The updraft is maximised downshear-left, while the rainfall is maximised to the left of shear. From Frank and Ritchie (2001).

to the shear leads to the penetration of dry air to the storm core in the lower to mid-troposphere, causing convective downdrafts that cool and dry the boundary layer. The combination of shear, dry air and the low-level inversion can lead to rapid destruction of hurricanes (Dunion and Velden, 2004). The importance of the combination of dry environmental air and shear was also recognised by Emanuel *et al.* (2004), who developed an empirical parameterisation of these effects for incorporation into an axisymmetric intensity prediction model.

Satellite remote-sensed temperature profiles show that the height of the warm core in hurricanes decreases as the environmental shear increases (Knaff *et al.*, 2004). The effect is not large, with the difference in height of the peak mean temperature anomaly between the low- ($<3.8\,\mathrm{m\,s^{-1}}$) and high-shear ($>6.8\,\mathrm{m\,s^{-1}}$) groups of about 1 km, although the coarse vertical resolution of the satellite sounder makes accurate estimation of the difference difficult. Nevertheless, the trend is consistent with the moist simulations discussed above, and particularly with Frank and Ritchie (2001)'s finding that storms in full-physics simulations weaken from the top down in environmental shear.

8.4. *Observations of the Convective Asymmetry*

Azimuthal variations in cloudiness and precipitation are a common and widely recognised symptom of the asymmetric vertical motion resulting from environmental vertical wind shear. Such asymmetries have been presented in case studies of individual storms, and are confirmed in surveys of large numbers of storms.

Detailed studies of the evolution of two hurricanes in sheared environments, Jimena (1991) and Olivia (1994) were presented by Black *et al.* (2002). At the start of the respective study periods, each storm had a small eye of 16–18 km radius, maximum winds of approximately $57\,\mathrm{m\,s^{-1}}$ and lay over SSTs in excess of 28°C. Jimena experienced two days of $13–20\,\mathrm{m\,s^{-1}}$ easterly shear, during which it maintained constant intensity or weakened slightly. Olivia intensified during a day of $8\,\mathrm{m\,s^{-1}}$ easterly shear, but weakened rapidly the following day as the shear reversed and increased to greater than $15\,\mathrm{m\,s^{-1}}$ from the west, and the storm moved over cooler water. The evolution of Olivia on the second day, over a period of about 3.5 hours during which the vertical shear over the inner core increased from 3–5 to $15\,\mathrm{m\,s^{-1}}$ over the lowest 10 km, was studied in detail by Reasor *et al.* (2000) and Black *et al.* (2002). The azimuthal-mean circulation dramatically weakened, especially at higher levels, and the RMW expanded. The radar reflectivity became markedly asymmetric, with peak reflectivities to the left of the vertical shear vector, consistent with a strong asymmetry that developed in the eyewall vertical motion with the maximum updraft to the downshear-left. The vortex tilt over the 0.75–6 km layer increased from zero to about 3 km. The eye became elliptical and trailing spirals of vorticity with azimuthal wavenumber 2 formed.

The convective structure in both storms was strongly influenced by the environmental shear. Jimena displayed a strong tendency for convection to be to the left of the shear vector on both days. Individual convective cells formed on the downshear side of the eyewall and propagated around to the left at 60–80% of the tangential wind velocity, consistent with VRW propagation. Most dissipated near the upshear side, although one long-lived cluster was tracked for a full circuit. The observed buoyant updrafts accelerated to the left of the shear vector, rising through the freezing level on the upshear side whereupon the hydrometeors fell out or froze, resulting in the decrease in reflectivity. On the right of shear, lower tropospheric precipitation-driven downdrafts lay beneath glaciated upper tropospheric updrafts. Olivia similarly displayed a relatively weak asymmetry while the shear was weak, with eyewall cells able to be tracked right around the eyewall. Outer convection was close to circular, and may have represented the beginnings of an eyewall replacement cycle. As the shear increased and the storm moved over colder water and weakened, the reflectivity in and outside of the eyewall became strongly asymmetric and individual eyewall cells became short-lived and confined to the left-of-shear semicircle. Figure 12 shows aircraft data from the storm at this stage. The strong left-of-shear radar reflectivity signature is highly characteristic of this situation, and is accompanied by maximum radial inflow and vertical motion at the downshear end of the eyewall.

Hurricane Norbert of 1984 (Marks *et al.*, 1992) similarly had a strong radar reflectivity asymmetry, with inner core precipitation predominantly to the left of the inner-core shear vector. The eyewall vertical motion was consistent with the rainfall structure, being upwards in the right-front quadrant, increasing to strongly upwards to the left, with descent to the rear and right. The earth-relative radial and azimuthal winds were kinematically equivalent to a front-to-back crossflow at 1-km height, reversing to back-to-front above 3 km, consistent with the shear structure, although the flow up to 3-km height also contained characteristics of the motion-induced boundary-layer

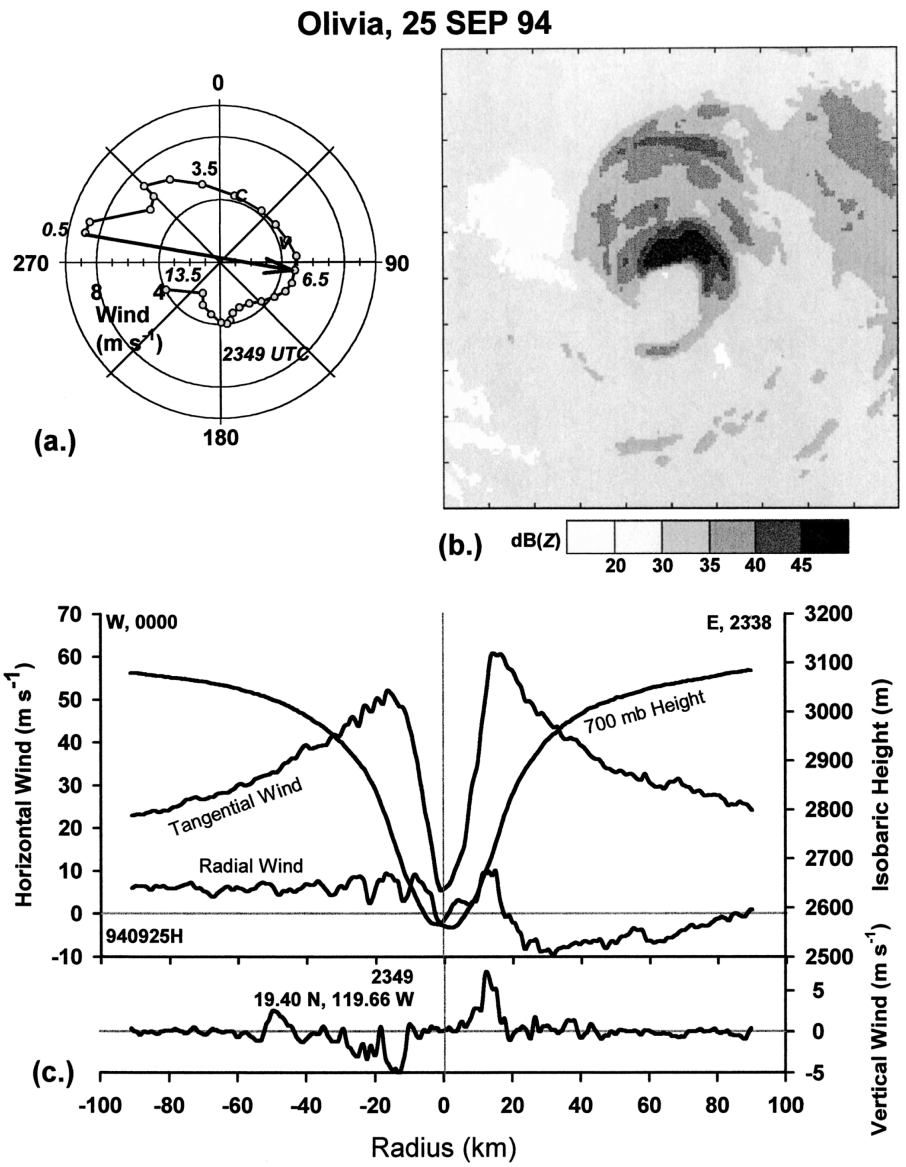

Figure 12. Hurricane Olivia late in the day on 25 Sep 1994: (a) Doppler-derived relative-wind hodograph, storm motion (C) and vertically-averaged earth-relative wind (V) at 2349 UTC. Winds are averaged over a 20–30 km storm-centred annulus. The arrow represents the largest shear. (b) Radar reflectivity PPI composite for 2338-2359 UTC, domain size is 240 k square. (c) An east-west profile of flight-level observations at 700 hPa, 2338–0000 UTC. From Black *et al.* (2002).

asymmetric flow (section 5). Hurricane Gloria of 1985 (Franklin *et al.*, 1993) similarly had the maximum updraft at 500 hPa on the downshear side of the eyewall, and descent on the upshear side. The eyewall radar reflectivity was a maximum in a band extending cyclonically from the updraft core to the downdraft; that is, predominantly on the left of the shear vector.

A more extensive survey of convective asymmetry, using lightning flash data as a proxy for convection, was conducted by Corbosiero and Molinari (2002, 2003). Lightning is strongly

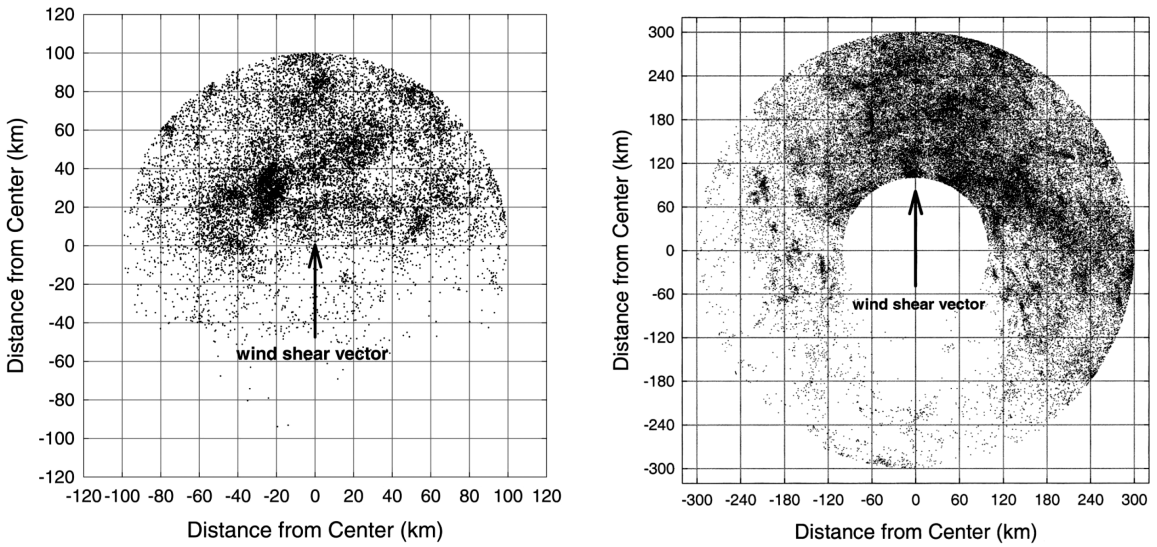

Figure 13. Locations of lightning flashes (left) within 100 km and (right) 100–300 km of the storm centres for environmental shear exceeding 10 m s^{-1}. The data have been rotated so that the wind shear vector is pointing upwards on the page. From Corbosiero and Molinari (2002).

correlated with the direction of the environmental shear. Over 90% of flashes occur in the downshear half of the storm once the shear exceeds 5 m s^{-1}. There is a slight preference for downshear left in the innermost 100 km, and a stronger preference for downshear right in the 100–300 km annulus, as shown in Fig. 13. The downshear-left preference in the core is more marked in more intense storms, probably because the strong rotation twists updrafts initiated downshear helically around to the left, then upshear, of the storm centre. In most of the storms, shear and the motion-induced frictional asymmetry (section 5) would place the convective maximum in similar quadrants, so it is difficult to separate the effects. In storms where the expected maxima were in different quadrants, the shear-induced asymmetry dominates that due to motion.

The rainfall asymmetry due to shear and storm motion, as measured by instruments on the TRMM satellite, was reported by Lonfat (2004) and Chen *et al.* (2006). A consistent downshear-left asymmetry is apparent (downshear-right in the southern hemisphere). It is similar to that in the lightning data of Corbosiero and Molinari (2003), except that the rain asymmetry is most marked for the weaker storms, and is downshear-left at all radii. The shear-induced asymmetry is reasonably independent of storm intensity for strong shear >7.5 m s^{-1}, but weaker shear <7.5 m s^{-1} impacts most strongly on less intense storms. The expected right-front motion-induced convective maximum (section 5.1.2) is swamped by the effects of shear when the shear is strong, but some signal remains for weak shear outside the storm inner core. The preferred downshear-right convection in the outer core often occurs in the form of a quasistationary, persistent "principal band", accompanied by weaker mobile "secondary bands" (Willoughby *et al.*, 1984).

Annular hurricanes (section 7.4), characterised partly by their unusually high degree of symmetry on satellite images, require weak polewards and westwards environmental shear for their formation (Knaff *et al.*, 2003). The environmental shear cancels out the β-gyre-induced shear over the core. They thus represent a null case for shear-induced convective asymmetry.

8.5. *Observations of Axis Tilt*

Actual observations of axis tilt through the depth of the troposphere in tropical cyclones are rare, due to the difficulty of obtaining sufficient data to locate a well-defined centre at multiple levels. The wind centre of Hurricane Norbert, located from airborne Doppler radar, described a roughly elliptical anticyclonic spiral with height, with long axis about 4 km oriented approximately along the inner core shear of about $10\,\mathrm{m\,s^{-1}}$ over 10 km (Marks *et al.*, 1992). Franklin *et al.* (1993) found that the centre of the very intense Hurricane Gloria had only slight displacement with height, in spite of significant environmental shear. The pressure centres of Hurricane Bonnie (1998), located from aircraft data at 850, 600 and 300 hPa and at the surface from dropsonde observations, displayed a surface — 300 hPa tilt of about 45 km oriented about 45° left of the environmental 850 — 200 hPa shear of $11.9\,\mathrm{m\,s^{-1}}$ (Kepert, 2005). Most of the tilt was between the 600 and 300 hPa levels, where the shear was also strongest. Simulation of this storm by Rogers *et al.* (2003) showed a similar but smaller tilt of about 15 km over the surface — 400 hPa layer, with the simulated rainfall asymmetry in good agreement with that observed by airborne radar. The agreement between observed and modelled tilt is reasonable, with the difference being partly because the observations are 6 hours earlier than the simulation, that the shear was slowly weakening, and that the model shear was presented over a thinner layer. Finally, Zehr (2003) compared aircraft and satellite-estimated centre positions of Hurricane Bertha at three levels. Initial tilts of up to 104 km, slightly to the left of the environmental shear, were diagnosed, although later in the period the upper-tropospheric tilt reversed while the shear only slowly weakened.

8.6. *Shear Associated with Upper-level Troughs*

Environmental shear generally results in a tropical cyclone weakening (section 8.3), except when the shear is due to an approaching upper trough. This situation is complex, and a trough may cause either weakening or strengthening depending on the particular circumstances. It can also be difficult to extract the trough effect from other intensity change influences. Nevertheless, this is an important situation, since the low inertial stability of the outflow layer provides an avenue whereby the environment can directly affect the core of the storm. In this section, we restrict attention to the case where the cyclone remains tropical after the interaction. The important process of extratropical transition is considered in Chapter 5.

Hurricane Elena (1985) twice experienced marked intensity changes, each about 30 hours after periods of significant upper level eddy flux of angular momentum (Molinari and Vollaro, 1989, 1990). Major intensification occurred following the passage of a mid-latitude trough polewards of the storm, which caused a large inwards angular momentum eddy flux. An in–up–out circulation, consisting of a thin upper tropospheric outflow and a deep inflow layer connected by a band of ascent, developed inwards of the momentum source, as predicted by balanced vortex theory (section 3), and propagated inwards. When it reached the core, a secondary wind maximum developed and contracted, resulting in an extended period of rapid intensification. A PV analysis of the event (Molinari *et al.*, 1995) showed that the trough interaction was not a simple superposition of the trough's PV over Elena's. Rather, the upper-level PV anomaly that eventually approached the centre was much narrower than the original trough because the outflow anticyclone of Elena contributed to synoptic-scale wave breaking, so that interaction with a substantial layer of vertical shear that might have prevented intensification was avoided. Moreover, the enhanced convection caused by these developments eroded the PV anomaly, and prevented weakening of the cyclone as it moved to the east. A similar mechanism occurred in Hurricane Danny (Molinari *et al.*, 1998).

The rapid intensification of Supertyphoon Flo was also linked to a period of enhanced eddy flux convergence of angular momentum, which preceded the rapid intensification by about a day. Titley and Elsberry (2000) characterise this phase as a preconditioning, in which a cyclonic wind burst develops above 200 hPa, decreasing the vertical shear near this level. The warm core moves upwards, and at 200 hPa the outflow increases, with inflow immediately below. These components are consistent with the upper level forcing of a balanced symmetric cyclone as discussed in section 3. They apparently developed in response to the eddy flux convergence of angular momentum and acted as a catalyst for the subsequent rapid intensification to a supertyphoon. The rapid intensification itself was apparently an internal readjustment of the storm, probably accompanied with an eyewall replacement cycle. It occurred during a period of declining upper level outflow and angular momentum forcing. Later, Flo underwent a similarly rapid weakening during a period of modest environmental wind shear, positive eddy flux convergence, warm SSTs, and vigorous outflow. The crucial difference appears to be that the angular momentum convergence extended downward to about 500 hPa. It is the vertical derivative of the momentum forcing that drives the secondary circulation (26), so this deep eddy flux convergence of angular momentum would have resulted in a deep secondary circulation, with lower-tropospheric heat release and relatively inefficient energy conversion. The rapid intensification of Flo can be contrasted to the much more modest evolution of Typhoons Ed (Titley and Elsberry, 2000) and Gene (Wu and Cheng, 1999), a comparison which emphasises the subtle variations in environmental forcing that often controls the pace and nature of intensity change.

The rapid intensifications of Hurricanes Bertha (1996) and Erin (2001) were analysed by Shapiro and Möller (2005), using piecewise PV inversion to isolate the effects of the trough. Bertha's intensification was directly augmented by a trough, but trough interaction did not contribute to Erin's intensification. Rather, other factors sufficed.

Hanley *et al.* (2001) surveyed 10 years of North Atlantic storms, and subdivided trough interactions according to whether the upper PV mass was closer than 400 km from the storm or further away, respectively "superposition" and "distant interaction" events. Each type of interaction can precede either intensification or weakening. Provided other unfavourable indicators, such as cold water or landfall, are absent, 78% of superposition cases intensify in the North Atlantic, soon after the small-scale upper tropospheric PV mass approaches the storm centre. In these cases, as in Hurricane Elena, the PV maximum weakens and never crosses the storm to produce weakening. Distant interaction leads to intensification in 61% of cases. In these situations, the upper PV maximum remains well to the west of the storm while strong upper-level divergence and a marked jet stream develop downshear. These features probably result from cooperative interaction between the systems. The maximum divergence and the equatorwards entrance region of the jet are located near the cyclone, leading to strong upwards motion that favours intensification. The differences between this case and that of unfavourable distant interaction are subtle, being largely a matter of a slightly stronger and larger PV maximum giving about $5\,\mathrm{m\,s^{-1}}$ more vertical shear over the cyclone.

A similar delicate balance of opposing effects was noted by DeMaria *et al.* (1993), who found that upper level eddy flux convergence of angular momentum was on its own unfavourable for intensification, due to the association with shear. However, when the effects of shear were separately accounted for in the regression, the eddy flux convergence had an intensifying effect, which was strongest at a lead time of 48 hours and within 600 km of the storm centre. This parameter was used as a predictor in SHIPS, the Statistical Hurricane Intensity Prediction Scheme, up until 2002. (DeMaria *et al.*, 2005).

The much-studied rapid intensification of Hurricane Opal (1995) provides an excellent example of the forecast and diagnosis difficulties. Several careful studies (Bosart *et al.*, 2000; Persing *et al.*, 2002; Möller and Shapiro, 2002; Shapiro and Möller, 2003) have analysed the role of the approaching upper trough without arriving at a consensus. Bosart *et al.* (2000) noted that upper-level divergence near the trough and jet extended equatorwards and coincided with Opal, just before an increase in convection and the onset of rapid intensification. Persing *et al.* (2002) and Möller and Shapiro (2002) identified positive eddy vorticity fluxes in the vicinity of Opal, but a balanced vortex calculation showed that the forcing of the intensification was dominated by the mean (i.e. symmetric) terms. Shapiro and Möller (2003) used piecewise potential vorticity inversion to isolate the effects of the upper-level trough. They likewise found no indication that it was a significant contributor to Opal's lower-tropospheric intensification. The diagnosis of Hurricane Opal was complicated by the fact that the rapid intensification began as or slightly before it passed over an oceanic warm core ring (Hong *et al.*, 2000; Shay *et al.*, 2000), which would have also contributed. The subsequent rapid weakening before landfall further highlighted the forecast challenges.

9. Summary

The fundamental view of tropical cyclone intensification as a cooperative process between the primary and secondary circulations has now stood for four decades, and continues to underpin our understanding of tropical cyclones. Potential intensity theories rest on this idea. Diagnosis the secondary circulation and its effects contributed to the discovery of eyewall contraction as the means by which most storms intensify, and to the eyewall replacement cycle as a means by which intensity can vary due to internal processes within the storm.

More recently, observations, theory and numerical simulation have combined to demonstrate that small-scale features such as vortex Rossby waves and eyewall mesovortices are common in the inner core of intense tropical cyclones. The details of the primary circulation determines the nature and extent of these features, while the secondary circulation can help create the necessary conditions. Their effects can include rapid changes in the inner-core structure of the tropical cyclone, implying that intensity forecasting will continue to be difficult.

The storm's environment has long been known to influence its development. The effects of upper trough interactions include the consequences of their modulation of the secondary circulation. Understanding of the effects of environmental shear has grown to include the dynamics of a tilted vortex, from both potential vorticity and vortex Rossby wave perspectives. Fine details of the vortex's primary structure are important to the response to shear. That response to shear can include intensity change, and marked asymmetries in vertical motion, cloud and rainfall.

Much of the inflow in the secondary circulation occurs in the boundary layer. The boundary layer is far from horizontally homogeneous, with marked variation in height and structure evident from observations. Theory and simulation have successfully explained these differences. The local boundary layer is strongly influenced by the details of the vortex primary structure and by position within the storm.

In spite of the overall complexity of the dynamics, tropical cyclones can be usefully described parametrically with relatively few parameters. As with other aspects of the atmosphere, the attractor is locally of low dimension.

In summary, tropical cyclone structure and intensity are sensitive to a variety of internal processes and external factors. Integrating these influences can be difficult in practice, and so it remains unclear what the ultimate limits of intensity and structure prediction are.

Table 2. Symbols and abbreviations used in this chapter.

Symbol	Meaning
b	Shape parameter in Holland vortex profile
c_p	Heat capacity of air at constant pressure
c_{pd}	c_p for dry air
d/dt	Total derivative, $d/dt = \partial/\partial t + u\,\partial/\partial r + v/r\,\partial/\partial\lambda + w\,\partial/\partial z$
e	Base of natural logarithms
f	Coriolis parameter
f_0	Coriolis parameter at cyclone centre
g	Gravitational acceleration
k	Radial wavenumber
k	Specific enthalpy
k_0	Radial wavenumber at $t = 0$
k_0^*	Saturation specific enthalpy at sea surface
n	Azimuthal wavenumber
p	Pressure
p_c	Central pressure
q	Specific humidity
$\overline{q'w'}$	Vertical turbulent flux of q
q_s	Saturation specific humidity
r	Radial coordinate
r_m	Radius of maximum wind
r^*	Critical radius for vortex Rossby waves
t	Time
u	Radial velocity
$\overline{u'w'}$	Vertical turbulent flux of u
$\overline{v'w'}$	Vertical turbulent flux of v
v	Azimuthal velocity
v_{gr}	Gradient wind
v_m	Maximum azimuthal wind
w	Vertical velocity
z	Height coordinate
B	Baroclinicity $g/\theta\,\partial\theta/\partial r$
C	Radial acceleration $v^2/r + fv$
C_D	Drag coefficient
C_E	Enthalpy transfer coefficient
E	Net evaporation rate (i.e. evaporation — condensation)
EPI	Potential intensity theory according to Emanuel
$\mathbf{F}$	Body force per unit mass (e.g. due to friction)
F_λ	Azimuthal component of $\mathbf{F}$
F_x, F_y	Horizontal components of $\mathbf{F}$
F_R	Rotational Froude number
H	Equivalent depth of the atmosphere
HPI	Potential intensity theory according to Holland
I	Inertial stability
L_R	Rossby deformation radius
L_v	Latent heat of vapourisation
M_a	Vertical component of absolute angular momentum
$\overline{M_a'w'}$	Vertical turbulent flux of M_a
N	Brunt-Väisälä frequency
PI	Potential intensity
PV	Potential vorticity
Q	Rossby-Ertel potential vorticity
R	Gas constant
R_d	Gas constant for dry air
RMW	Radius of maximum wind
SWF	Surface wind factor
T	Temperature
T_o	Outflow temperature
T_s	Surface temperature
T_v	Virtual temperature
VRW	Vortex Rossby wave
β	Meridional gradient of f
Δp	Central pressure deficit
ϵ	Ratio of molecular weight of water to that of dry air
ζ	Relative vorticity
$\overline{\zeta}_0$	Relative vorticity of basic-state vortex
$\overline{\zeta}_0'$	Radial derivative of $\overline{\zeta}_0$
η	Vertical component of absolute vorticity
$\boldsymbol{\eta}$	Absolute vorticity vector
θ	Potential temperature
$\dot{\theta}$	Diabatic heating rate
θ_e	Equivalent potential temperature
θ_e^*	Saturation equivalent potential temperature
θ_v	Virtual potential temperature
$\overline{\theta'w'}$	Vertical turbulent flux of θ
λ	Azimuth, measured anticlockwise from the positive x-axis
ξ	Inertia parameter
ρ	Air density in height coordinates (i.e. SI units of $\mathrm{kg\,m^{-3}}$)
ρ_{parcel}	Density of air parcel
ρ_{ref}	Density of reference atmospheric profile
σ	Air density in isentropic coordinates (i.e. SI units of $\mathrm{kg\,m^{-2}K^{-1}}$)
ω	Frequency
$\overline{\Omega}_0$	Angular velocity of basic-state vortex
$\overline{\Omega}_0'$	Radial derivative of $\overline{\Omega}_0$
∇	del operator of differential vector calculus
$\nabla_\theta\cdot$	Horizontal divergence in isentropic coordinates

Acknowledgements

In preparing this chapter, I drew on the earlier chapters by Holland (1987) and Willoughby (1995), and the excellent efforts of the various topic chairs and research rapporteurs at the 4th, 5th and 6th International Workshops on Tropical Cyclones, including Kerry Emanuel,

Russell Elsberry, Greg Holland, John Knaff, Frank Marks, John Molinari, Liz Ritchie, Roger Smith, and Hugh Willoughby. The opinions expressed by the author in this chapter are scientifically based and are personal opinions. They are not an expression of Australian Government policy.

References

Aberson, S. D., M. T. Montgomery, M. Bell, and M. Black, 2006: Hurricane Isabel (2003): New insights into the physics of intense storms. Part II: Extreme localized wind. *Bull. Amer. Meteor. Soc.*, **86**, 1349–1354.

Barnes, G. M. and P. B. Bogner, 2001: Comments on "surface observations in the hurricane environment". *Mon. Wea. Rev.*, **129**, 1267–1269.

Barnes, G. M. and M. D. Powell, 1995: Evolution of the inflow boundary layer of Hurricane Gilbert (1988). *Mon. Wea. Rev.*, **123**, 2348–2368.

Barnes, G. M., E. J. Zipser, D. Jorgensen, and F. D. Marks, Jr., 1983: Mesoscale and convective structure of a hurricane rainband. *J. Atmos. Sci.*, **40**, 2125–2137.

Bell, M. M. and M. T. Montgomery, 2008: Observed structure, evolution and potential intensity of category five Hurricane Isabel (2003) from 12–14 September. *Mon. Wea. Rev.*, **136**, 2023–2046.

Bister, M. and K. A. Emanuel, 1998: Dissipative heating and hurricane intensity. *Meteorol. Atmos. Phys.*, **50**, 233–240.

Black, M. L., R. W. Burpee, and F. D. Marks, Jr., 1996: Vertical motion characteristics of tropical cyclones determined with airborne Doppler radial velocities. *J. Atmos. Sci.*, **53**, 1887–1909.

Black, M. L., J. F. Gamache, F. D. Marks, Jr., C. E. Samsury, and H. E. Willoughby, 2002: Eastern Pacific Hurricanes Jimena of 1991 and Olivia of 1994: The effect of vertical shear on structure and intensity. *Mon. Wea. Rev.*, **130**, 2291–2312.

Black, P. G., R. L. Elsberry, L. K. Shay, R. P. Partridge, and J. Hawkins, 1988: Atmospheric boundary layer and oceanic mixed layer observations in Hurricane Josephine from air-deployed drifting buoys and research aircraft. *J. Atmos. Ocean. Tech.*, **5**, 683–698.

Black, P. G. and F. D. Marks, 1991: The structure of an eyewall meso-vortex in Hurricane Hugo (1989). *Preprints, 19th Conf. on Hurricanes and Tropical Meteorology*, Miami, FL, *Amer. Meteor. Soc.*, 579–582.

Bosart, L. F., C. S. Velden, W. E. Bracken, J. Molinari, and P. G. Black, 2000: Environmental influences on the rapid intensification of Hurricane Opal (1995) over the Gulf of Mexico. *Mon. Wea. Rev.*, **128**, 322–352.

Braun, S. A., 2002: A cloud-resolving simulation of Hurricane Bob (1991): Storm structure and eyewall buoyancy. *Mon. Wea. Rev.*, **130**, 1573–1592.

Braun, S. A., M. T. Montgomery, and Z. Pu, 2006: High-resolution simulation of Hurricane Bonnie (1998). Part I: The organization of eyewall vertical motion. *J. Atmos. Sci.*, **63**, 19–42.

Bryan, G. H. and R. Rotunno, 2009a: The influence of near-surface, high-entropy air in hurricane eyes on maximum hurricane intensity. *J. Atmos. Sci.*, **66**, 148–158.

———, 2009b: The maximum intensity of tropical cyclones in axisymmetric numerical model simulations. *Mon. Wea. Rev.*, **137**, 1770–1789.

Camp, J. P. and M. T. Montgomery, 2001: Hurricane maximum intensity: Past and present. *Mon. Wea. Rev.*, **129**, 1704–1717.

Carr, L. E., III and R. T. Williams, 1989: Barotropic vortex stability to perturbations from axisymmetry. *J. Atmos. Sci.*, **46**, 3177–3191.

Carrier, G. F., 1971: Swirling flow boundary layers. *J. Fluid. Mech.*, **49**, 133–144.

Charney, J. G. and A. Eliassen, 1964: On the growth of the hurricane depression. *J. Atmos. Sci.*, **21**, 68–75.

Chen, S. S., J. A. Knaff, and F. D. Marks, Jr., 2006: Effects of vertical wind shear and storm motion on tropical cyclone rainfall asymmetries deduced from TRMM. *Mon. Wea. Rev.*, **134**, 3190–3208.

Chen, Y., G. Brunet, and M. K. Yau, 2003: Spiral bands in a simulated hurricane. Part II: Wave activity diagnostics. *J. Atmos. Sci.*, **60**, 1239–1256.

Chen, Y. and M. K. Yau, 2001: Spiral bands in a simulated hurricane. Part I: Vortex Rossby wave verification. *J. Atmos. Sci.*, **58**, 2128–2145.

Cione, J. J., P. G. Black, and S. H. Houston, 2000: Surface observations in the hurricane environment. *Mon. Wea. Rev.*, **128**, 1550–1561.

Corbosiero, K. L. and J. Molinari, 2002: The effects of vertical wind shear on the distribution of convection in tropical cyclones. *Mon. Wea. Rev.*, **130**, 2110–2123.

———, 2003: The relationship between storm motion, vertical wind shear, and convective asymmetries in tropical cyclones. *J. Atmos. Sci.*, **60**, 366–376.

Corbosiero, K. L., J. Molinari, and A. R. Aiyyer, 2006: The structure and evolution of Hurricane Elena (1985). Part II: Convective asymmetries and evidence for vortex-Rossby waves. *Mon. Wea. Rev.*, **134**, 3073–3091.

Cram, T. A., J. Persing, M. T. Montgomery, and S. A. Braun, 2007: A Lagrangian trajectory view on transport and mixing processes between the eye, eyewall, and environment using a high-resolution simulation of Hurricane Bonnie (1998). *J. Atmos. Sci.*, **64**, 1835–1856.

DeMaria, M., J.-J. Baik, and J. Kaplan, 1993: Upper-level eddy angular momentum fluxes and tropical cyclone intensity change. *J. Atmos. Sci.*, **50**, 1133–1147.

DeMaria, M. and J. Kaplan, 1994: A statistical hurricane intensity prediction scheme (SHIPS) for the Atlantic basin. *Wea. Forecasting*, **9**, 209–220.

———, 1999: An updated statistical hurricane intensity prediction scheme (SHIPS) for the Atlantic and eastern North Pacific basins. *Wea. Forecasting*, **14**, 326–337.

DeMaria, M., M. Mainelli, L. K. Shay, J. A. Knaff, and J. Kaplan, 2005: Further improvements to the Statistical Hurricane Intensity Prediction Scheme (SHIPS). *Wea. Forecasting*, **20**, 531–543.

Dunion, J. P. and C. S. Velden, 2004: The impact of the Saharan air layer on Atlantic tropical cyclone activity. *Bull. Amer. Meteor. Soc.*, **85**, 353–365.

Eastin, M. D., W. M. Gray, and P. G. Black, 2005a: Buoyancy of convective vertical motions in the inner core of intense hurricanes. Part I: General statistics. *Mon. Wea. Rev.*, **133**, 188–208.

———, 2005b: Buoyancy of convective vertical motions in the inner core of intense hurricanes. Part II: Case studies. *Mon. Wea. Rev.*, **133**, 209–227.

Eliassen, A., 1971: On the Ekman layer in a circular vortex. *J. Met. Soc. Japan*, **49**, 784–789.

Eliassen, A. and M. Lystad, 1977: The Ekman layer of a circular vortex. A numerical and theoretical study. *Geophysica Norvegica*, **7**, 1–16.

Emanuel, K. A., 1986: An air-sea interaction theory for tropical cyclones. Part I: Steady-state maintenance. *J. Atmos. Sci.*, **43**, 585–604.

———, 1988: The maximum intensity of hurricanes. *J. Atmos. Sci.*, **45**, 1143–1155.

———, 1994: *Atmospheric Convection*. Oxford University Press, 580 pp.

———, 1995: Sensitivity of tropical cyclones to surface exchange coefficients and a revised steady-state model incorporating eye dynamics. *J. Atmos. Sci.*, **52**, 3969–3976.

———, 1997: Some aspects of hurricane inner-core dynamics and energetics. *J. Atmos. Sci.*, **54**, 1014–1026.

———, 2000: A statistical analysis of tropical cyclone intensity. *Mon. Wea. Rev.*, **128**, 1139–1152.

———, 2003: Tropical cyclones. *Annu. Rev. Earth Planet. Sci.*, **31**, 75–104.

Emanuel, K. A., C. DesAutels, C. Holloway, and R. Korty, 2004: Environmental control of tropical cyclone intensity. *J. Atmos. Sci.*, **61**, 843–858.

Etling, D. and R. A. Brown, 1993: Roll vortices in the planetary boundary layer: A review. *Boundary Layer Meteorology*, **65**, 215–248.

Foster, R. C., 2005: Why rolls are prevalent in the hurricane boundary layer. *J. Atmos Sci.*, **62**, 2647–2661.

Frank, W. M. and E. A. Ritchie, 1999: Effects of environmental flow upon tropical cyclone structure. *Mon. Wea. Rev.*, **127**, 2044–2061.

———, 2001: Effects of vertical wind shear on the intensity and structure of numerically simulated hurricanes. *Mon. Wea. Rev.*, **129**, 2249–2269.

Franklin, J. L., M. L. Black, and K. Valde, 2003: GPS dropwindsonde wind profiles in hurricanes and their operational implications. *Wea. Forecasting*, **18**, 32–44.

Franklin, J. L., S. J. Lord, S. E. Feuer, and F. D. Marks, Jr., 1993: The kinematic structure of Hurricane Gloria (1985) determined from nested analyses of dropwindsonde and Doppler radar data. *Mon. Wea. Rev.*, **121**, 2433–2451.

Gall, R., J. Tuttle, and P. Hildebrand, 1998: Small-scale spiral bands observed in Hurricanes Andrew, Hugo, and Erin. *Mon. Wea. Rev.*, **126**, 1749–1766.

Gallina, G. M. and C. S. Velden, 2002: Environmental vertical wind shear and tropical cyclone intensity change utilizing enhanced satellite derived wind information. *Extended abstracts, 25th Conference on Hurricanes and Tropical Meteorology*, Amer. Meteorol. Soc., San Diego, CA, 29 April–3 May, pp. 172–173.

Gill, A. E., 1982: *Atmosphere–Ocean Dynamics*. Academic Press, 662 pp.

Guinn, T. A. and W. H. Schubert, 1993: Hurricane spiral bands. *J. Atmos. Sci.*, **50**, 3380–3403.

Hack, J. J. and W. H. Schubert, 1986: Nonlinear response of atmospheric vortices to heating by organised cumulus convection. *J. Atmos. Sci.*, **43**, 1559–1573.

Halverson, J. B., J. Simpson, G. Heymsfield, H. Pierce, T. Hock, and L. Ritchie, 2006: Warm core structure of Hurricane Erin diagnosed

from high altitude dropsondes during CAMEX-4. *J. Atmos. Sci.*, **63**, 309–324.

Hanley, D., J. Molinari, and D. Keyser, 2001: A composite study of the interactions between tropical cyclones and upper-tropospheric troughs. *Mon. Wea. Rev.*, **129**, 2570–2584.

Haurwitz, B., 1935: The height of tropical cyclones and the eye of the storm. *Mon. Wea. Rev.*, **63**, 45–49.

Haynes, P. H. and M. E. McIntyre, 1987: On the evolution of vorticity and potential vorticity in the presence of diabatic heating and frictional or other forces. *J. Atmos. Sci.*, **44**, 828–841.

———, 1990: On the conservation and impermeability theorems for potential vorticity. *J. Atmos. Sci.*, **47**, 2021–2031.

Holland, G. J., 1980: An analytic model of the wind and pressue profiles in hurricanes. *Mon. Wea. Rev.*, **108**, 1212–1218.

———, 1987: Mature structure and structure change. *A Global View Of Tropical Cyclones*, Elsberry, R. L., Ed., Office of Naval Research, pp. 13–52.

———, 1997: The maximum potential intensity of tropical cyclones. *J. Atmos. Sci.*, **54**, 2519–2541.

Holland, G. J. and R. T. Merrill, 1984: On the dynamics of tropical cyclone structural changes. *Quart. J. Roy. Meteor. Soc.*, **110**, 723–745.

Hong, X., S. W. Chang, S. Raman, L. K. Shay, and R. Hodur, 2000: The interaction between Hurricane Opal (1995) and a warm core ring in the Gulf of Mexico. *Mon. Wea. Rev.*, **128**, 1347–1365.

Hoskins, B. J., M. E. McIntyre, and A. Robertson, 1985: On the use and significance of isentropic potential vorticity maps. *Quart. J. Roy. Meteor. Soc.*, **111**, 877–946.

Jones, S. C., 1995: The evolution of vortices in vertical shear. Part I: Initially barotropic vortices. *Quart. J. Roy. Meteor. Soc.*, **121**, 821–851.

———, 2000a: The evolution of vortices in vertical shear. II: Large-scale asymmetries. *Quart. J. Roy. Meteor. Soc.*, **126**, 3137–3160.

———, 2000b: The evolution of vortices in vertical shear. III: Baroclinic vortices. *Quart. J. Roy. Meteor. Soc.*, **126**, 3161–3186.

Jorgensen, D. P., E. J. Zipser, and M. A. LeMone, 1985: Vertical motions in intense hurricanes. *J. Atmos. Sci.*, **42**, 839–856.

Katsaros, K. B., P. W. Vachon, W. T. Liu, and P. G. Black, 2002: Microwave remote sensing of tropical cyclones from space. *J. Oceanogr.*, **58**, 137–151.

Kepert, J. D., 2001: The dynamics of boundary layer jets within the tropical cyclone core. Part I: Linear theory. *J. Atmos. Sci.*, **58**, 2469–2484.

———, 2002a: An analysis of some tropical cyclone boundary layer wind observations. *Extended abstracts, 25th Conference on Hurricanes and Tropical Meteorology*, Amer. Meteor. Soc., San Diego, California, 29 April–3 May, pp. 615–616.

———, 2002b: Modelling the tropical cyclone boundary layer wind-field at landfall. *Extended abstracts, 14th BMRC Modelling Workshop: Modelling and Predicting Extreme Events, Melbourne, Australia, 11-13 November*, Hollis, A. J. and P. J. Meighen, Eds., Bureau of Meteorology Research Centre, pp. 81–84.

———, 2002c: The Wind-Field Structure of the Tropical Cyclone Boundary-Layer. Ph.D. thesis, Department of Mathematics and Statistics, Monash University.

———, 2005: Objective analysis of tropical cyclone location and motion from high density observations. *Mon. Wea. Rev.*, **133**, 2406–2421.

———, 2006a: Observed boundary–layer wind structure and balance in the hurricane core. Part I: Hurricane Georges. *J. Atmos. Sci.*, **63**, 2169–2193.

———, 2006b: Observed boundary–layer wind structure and balance in the hurricane core. Part II: Hurricane Mitch. *J. Atmos. Sci.*, **63**, 2194–2211.

Kepert, J. D. and Y. Wang, 2001: The dynamics of boundary layer jets within the tropical cyclone core. Part II: Nonlinear enhancement. *J. Atmos. Sci.*, **58**, 2485–2501.

Kimball, S. K. and J. L. Evans, 2002: Idealized simulations of hurricane-trough interaction. *Mon. Wea. Rev.*, **130**, 2210–2227.

Knaff, J. A., T. A. Cram, A. B. Schumacher, J. P. Kossin, and M. DeMaria, 2008: Objective identification of annular hurricanes. *Wea. Forecasting*, **23**, 17–28.

Knaff, J. A., J. P. Kossin, and M. DeMaria, 2003: Annular hurricanes. *Wea. Forecasting*, **18**, 204–223.

Knaff, J. A., S. A. Seseske, M. DeMaria, and J. L. Demuth, 2004: On the influences of vertical wind shear on symmetric tropical cyclone structure derived from AMSU. *Mon. Wea. Rev.*, **132**, 2503–2510.

Knupp, K. R., J. Walters, and M. Biggerstaff, 2005: Doppler profiler and radar observations of boundary layer variability during the landfall of tropical storm Gabrielle. *J. Atmos. Sci.*, **63**, 234–251.

Knupp, K. R., J. Walters, and E. W. M. Jr, 2000: Doppler profiler observations of Hurricane Georges at landfall. *Geophys. Res. Lett.*, **27**, 3361–3364.

Kossin, J. P. and M. D. Eastin, 2001: Two distinct regimes in the kinematic and thermodynamic structure of the hurricane eye and eyewall. *J. Atmos. Sci.*, **58**, 1079–1090.

Kossin, J. P. and W. H. Schubert, 2001: Mesovortices, polygonal flow patterns, and rapid pressure falls in hurricane-like vortices. *J. Atmos. Sci.*, **58**, 2196–2209.

———, 2003: Diffusion versus advective rearrangement of a circular vortex sheet. *J. Atmos. Sci.*, **60**, 586–589.

———, 2005: Mesovortices in Hurricane Isabel. *Bull. Amer. Meteor. Soc.*, **85**, 151–153.

Kuo, H.-C., L.-Y. Lin, C.-P. Chang, and R. T. Williams, 2004: The formation of concentric vorticity structures in typhoons. *J. Atmos. Sci.*, **61**, 2722–2734.

Kuo, H. L., 1971: Axisymmetric flow in the boundary layer of a maintained vortex. *J. Atmos. Sci.*, **28**, 20–41.

———, 1982: Vortex boundary layer under quadratic surface stress. *Boundary-Layer Meteorol.*, **22**, 151–169.

Kusunoki, K. and W. Mashiko, 2006: Doppler radar investigations of the inner core of Typhoon Songda (2004): Polygonal/elliptical eyewalls, eye contraction, and small-scale spiral bands. *Extended Abstracts, 27th Conference on Hurricanes and Tropical Meteorology*, Amer. Meteor. Soc., Monterey, CA, 24–28 April, CD–ROM.

Lonfat, M., 2004: Tropical Cyclone Rainfall: An Observational and Numerical Study of the Structure and Governing Physical Processes. Ph.D. thesis, Rosenthiel School of Marine and Atmospheric Sciences, University of Miami.

Lonfat, M., R. Rogers, T. Marchok, and F. D. Marks, Jr., 2007: A parametric model for predicting hurricane rainfall. *Mon. Wea. Rev.*, **135**, 3086–3097.

Lorsolo, S., J. L. Schroeder, P. Dodge, and F. D. Marks, Jr., 2008: An observational study of hurricane boundary layer small-scale coherent structures. *Mon. Wea. Rev.*, **136**, 2871–2893.

MacDonald, N. J., 1968: The evidence for the existence of Rossby-like waves in the hurricane vortex. *Tellus*, **20**, 138–150.

Mallen, K. J., M. T. Montgomery, and B. Wang, 2005: Reexamining the near core radial structure of the tropical cyclone primary circulation: Implications for vortex resiliency. *J. Atmos. Sci.*, **62**, 408–425.

Mallett, W. A., 2000: The Dynamics of the Atmospheric Boundary Layer of a Mature Tropical Cyclone: A Numerical Investigation. Ph.D. thesis, James Cook University, Australia.

Marks, F. D., P. G. Black, M. T. Montgomery, and R. W. Burpee, 2008: Structure of the eye and eyewall of Hurricane Hugo (1989). *Mon. Wea. Rev.*, **136**, 1237–1259.

Marks, F. D., Jr. and P. G. Black, 1990: Close encounter with an intense mesoscale vortex within Hurricane Hugo (September 15, 1989). *Extended Abstracts, Fourth Conf. on Mesoscale Processes*, Amer. Meteor. Soc., Boulder, CO, pp. 114–115.

Marks, F. D., Jr., P. Dodge, and C. Sandin, 1999: Observations of hurricane atmospheric boundary layer structure at landfall. *Extended abstracts, 23rd Conference on Hurricanes and Tropical Meteorology*, Amer. Meteorol. Soc., Dallas, TX, Jan. 10-15, pp. 1051–1055.

Marks, F. D., Jr., R. A. Houze, and J. F. Gamache, 1992: Dual-aircraft investigation of the inner core of Hurricane Norbert. Part I: Kinematic structure. *J. Atmos. Sci.*, **49**, 919–942.

May, P. T. and G. J. Holland, 1999: The role of potential vorticity generation in tropical cyclone rainbands. *J. Atmos. Sci.*, **56**, 1224–1228.

May, P. T., J. D. Kepert, and T. D. Keenan, 2008: Polarimetric radar observations of the persistently asymmetric structure of Tropical Cyclone Ingrid. *Mon. Wea. Rev.*, **136**, 616–630.

Maynard, R. H., 1945: Radar and weather. *J. Meteor.*, **2**, 214–226.

McWilliams, J. C., L. P. Graves, and M. T. Montgomery, 2003: A formal theory for vortex Rossby waves and vortex evolution. *Geophys. Astrophys. Fluid Dyn.*, **97**, 275–309.

Melander, M. V., J. C. McWilliams, and N. J. Zabusky, 1987: Axisymmetrization and vorticity-gradient intensification of an isolated two-dimensional vortex through filamentation. *J. Fluid Mech.*, **178**, 137–159.

Molinari, J., S. Skubis, and D. Vollaro, 1995: External influences on hurricane intensity. Part III: Potential vorticity evolution. *J. Atmos. Sci.*, **52**, 3593–3606.

Molinari, J., S. Skubis, D. Vollaro, F. Alsheimer, and H. E. Willoughby, 1998: Potential vorticity analysis of tropical cyclone intensification. *J. Atmos. Sci.*, **55**, 2632–2644.

Molinari, J. and D. Vollaro, 1989: External influences on hurricane intensity. Part I: Outflow layer eddy momentum fluxes. *J. Atmos. Sci.*, **46**, 1093–1105.

———, 1990: External influences on hurricane intensity. Part II: Vertical structure and response to the hurricane vortex. *J. Atmos. Sci.*, **47**, 1902–1918.

Möller, J. D. and M. T. Montgomery, 1999: Vortex Rossby waves and hurricane intensification in a barotropic model. *J. Atmos. Sci.*, **56**, 1674–1687.

———, 2000: Tropical cyclone evolution via potential vorticity anomalies in a three-dimensional balance model. *J. Atmos. Sci.*, **57**, 3366–3387.

Möller, J. D. and L. Shapiro, 2002: Balanced contributions to the intensification of Hurricane Opal as diagnosed from a GFDL model forecast. *Mon. Wea. Rev.*, **130**, 1866–1881.

Montgomery, M. T., M. M. Bell, S. D. Aberson, and M. L. Black, 2006: Hurricane Isabel (2003): New insights into the physics of intense storms. Part I. *Bull. Amer. Meteor. Soc.*, **86**, 1335–1347.

Montgomery, M. T. and R. J. Kallenbach, 1997: A theory of vortex Rossby waves and its application to spiral bands and intensity changes in hurricanes. *Quart. J. Roy. Meteor. Soc.*, **123**, 435–465.

Montgomery, M. T., H. D. Snell, and Z. Yang, 2001: Axisymmetric spindown dynamics of hurricane-like vortices. *J. Atmos. Sci.*, **58**, 421–435.

Montgomery, M. T., V. A. Vladimirov, and P. V. Denissenko, 2002: An experimental study on hurricane mesovortices. *J. Fluid Mech.*, **471**, 1–32.

Morrison, I., S. Businger, F. D. Marks, Jr., P. Dodge, and J. Businger, 2005: An observational case for the prevalence of roll vortices in the hurricane boundary layer. *J. Atmos. Sci.*, **62**, 2662–2673.

Moss, M. S. and S. L. Rosenthal, 1975: On the estimation of planetary boundary layer variables in mature hurricanes. *Mon. Wea. Rev.*, **103**, 980–988.

Muramatsu, T., 1986: The structure of polygonal eye of a typhoon. *J. Meteor. Soc. Japan*, **64**, 913–921.

Nolan, D. S., 2005: Instabilities in hurricane-like boundary layers. *Dynamics of Atmospheres and Oceans*, **40**, 209–236.

Nolan, D. S. and B. F. Farrell, 1999: The intensification of two-dimensional swirling flows by stochastic asymmetric forcing. *J. Atmos. Sci.*, **56**, 3937–3962.

Nolan, D. S. and L. D. Grasso, 2003: Nonhydrostatic, three-dimensional perturbations to balanced, hurricane-like vortices. Part II: Symmetric response and nonlinear simulations. *J. Atmos. Sci.*, **60**, 2717–2745.

Nolan, D. S. and M. T. Montgomery, 2000: The algebraic growth of wavenumber one disturbances in hurricane-like vortices. *J. Atmos. Sci.*, **57**, 3514–3538.

Nolan, D. S., M. T. Montgomery, and L. D. Grasso, 2001: The wavenumber-one instability and trochoidal motion of hurricane-like vortices. *J. Atmos. Sci.*, **58**, 3243–3270.

Nolan, D. S., Y. Moon, and D. P. Stern, 2007: Tropical cyclone intensification from asymmetric convection: energetics and efficiency. *J. Atmos. Sci.*, **64**, 3377–3405.

Nong, S. and K. Emanuel, 2003: A numerical study of the genesis of concentric eyewalls in hurricanes. *Quart. J. Roy. Meteor. Soc.*, **129**, 3323–3338.

Ooyama, K. V., 1964: A dynamical model for the study of tropical cyclone development. *Geofis. Intern.*, **4**, 187–198.

———, 1969: Numerical simulation of the life cycle of tropical cyclones. *J. Atmos. Sci.*, **26**, 3–40.

———, 1982: Conceptual evolution of the theory and modelling of the tropical cyclone. *J. Meteor. Soc. Japan*, **60**, 369–380.

Paterson, L. A., B. N. Hanstrum, N. E. Davidson, and H. C. Weber, 2005: Influence of environmental vertical wind shear on the intensity of hurricane-strength tropical cyclones in the Australian region. *Mon. Wea. Rev.*, **133**, 3644–3660.

Pendergrass, A. G. and H. E. Willoughby, 2009: Diabatically induced secondary flows in tropical cyclones. Part I: Quasi-steady forcing. *Mon. Wea. Rev.*, **137**, 805–821.

Peng, M. S., B.-F. Jeng, and R. T. Williams, 1999: A numerical study on tropical cyclone intensification. Part I: Beta effect and mean flow effect. *J. Atmos. Sci.*, **56**, 1404–1423.

Persing, J. and M. T. Montgomery, 2003: Hurricane superintensity. *J. Atmos. Sci.*, **60**, 2349–2371.

Persing, J., M. T. Montgomery, and R. E. Tuleya, 2002: Environmental interactions in the GFDL hurricane model for Hurricane Opal. *Mon. Wea. Rev.*, **130**, 298–317.

Pfeffer, R. L. and M. Challa, 1981: A numerical study of the role of eddy fluxes of momentum in the development of Atlantic hurricanes. *J. Atmos. Sci.*, **38**, 2393–2398.

———, 1992: The role of environmental asymmetries in Atlantic hurricane formation. *J. Atmos. Sci.*, **49**, 1051–1059.

Powell, M. D., 1980: Evaluation of diagnostic marine boundary-layer models applied to hurricanes. *Mon. Wea. Rev.*, **108**, 757–765.

———, 1982: The transition of the Hurricane Frederic boundary-layer wind field from the open Gulf of Mexico to landfall. *Mon. Wea. Rev.*, **110**, 1912–1932.

———, 1990a: Boundary layer structure and dynamics in outer hurricane bands. Part I:

Mesoscale rainfall and kinematic structure. *Mon. Wea. Rev.*, **118**, 891–917.

———, 1990b: Boundary layer structure and dynamics in outer hurricane bands. Part II: Downdraft modification and mixed layer recovery. *Mon. Wea. Rev.*, **118**, 918–938.

Powell, M. D. and P. G. Black, 1990: The relationship of hurricane reconnaissance flight-level wind measurements to winds measured by NOAA's oceanic platforms. *J. Wind Eng. Ind. Aero.*, **36**, 381–392.

Powell, M. D. and S. H. Houston, 1998: Surface wind fields of 1995 Hurricane Erin, Opal, Luis, Marilyn, and Roxanne at landfall. *Wea. Forecasting*, **11**, 1259–1273.

Powell, M. D., E. W. Uhlhorn, and J. D. Kepert, 2009: Estimating maximum surface winds from hurricane reconnaissance measurements. *Wea. Forecasting*, **24**, 868–883, doi:10.1175/2008WAF2007087.1.

Powell, M. D., P. J. Vickery, and T. A. Reinhold, 2003: Reduced drag coefficient for high wind speeds in tropical cyclones. *Nature*, **422**, 279–283.

Raymond, D. J., 1992: Nonlinear balance and potential-vorticity thinking at large Rossby number. *Quart. J. Roy. Meteor. Soc.*, **118**, 987–1015.

Reasor, P. D. and M. T. Montgomery, 2001: Three-dimensional alignment and corotation of weak, TC-like vortices via linear vortex Rossby waves. *J. Atmos. Sci.*, **58**, 2306–2330.

Reasor, P. D., M. T. Montgomery, and L. D. Grasso, 2004: A new look at the problem of tropical cyclones in vertical shear flow: Vortex resiliency. *J. Atmos. Sci.*, **61**, 3–22.

Reasor, P. D., M. T. Montgomery, F. D. Marks, Jr., and J. F. Gamache, 2000: Low-wavenumber structure and evolution of the hurricane inner core observed by airborne dual-Doppler radar. *Mon. Wea. Rev.*, **128**, 1653–1680.

Ritchie, E. A. and W. M. Frank, 2007: Interactions between simulated tropical cyclones and an environment with a variable Coriolis parameter. *Mon. Wea. Rev.*, **135**, 1889–1905.

Ritchie, E. A. and G. J. Holland, 1993: On the interaction of tropical-cyclone-scale vortices. II: Discrete vortex patches. *Quart. J. Roy. Meteor. Soc.*, **119**, 1363–1379.

Rogers, R., S. Chen, J. Tenerelli, and H. Willoughby, 2003: A numerical study of the impact of vertical shear on the distribution of rainfall in Hurricane Bonnie (1998). *Mon. Wea. Rev.*, **131**, 1577–1599.

Romine, G. S. and R. B. Wilhelmson, 2006: Finescale spiral band features within a numerical simulation of Hurricane Opal (1995). *Mon. Wea. Rev.*, **134**, 1121–1139.

Rosenthal, S. L., 1962: A theoretical analysis of the field of motion in the hurricane boundary layer. National hurricane research project report no. 56, U. S. Department of Commerece.

———, 1971: The response of a tropical cyclone model to variations in boundary layer parameters, initial conditions, lateral boundary conditions, and domain size. *Mon. Wea. Rev.*, **99**, 767–777.

Rozoff, C. M., W. H. Schubert, and B. D. McNoldy, 2006: Rapid filamentation zones in intense tropical cyclones. *J. Atmos. Sci.*, **63**, 325–340.

Ryan, B. F., G. M. Barnes, and E. J. Zipser, 1992: A wide rainband in a developing tropical cyclone. *Mon. Wea. Rev.*, **120**, 431–447.

Samsury, C. E. and E. J. Zipser, 1995: Secondary wind maxima in hurricanes: Airflow and relationship to rainbands. *Mon. Wea. Rev.*, **123**, 3502–3517.

Schecter, D. A. and M. T. Montgomery, 2004: Damping and pumping of a vortex Rossby wave in a monotonic cyclone: Critical layer stirring versus inertia-buoyancy wave emission. *Phys. Fluids*, **16**, 1334–1348.

———, 2007: Waves in a cloudy vortex. *J. Atmos. Sci.*, **64**, 314–337.

Schecter, D. A., M. T. Montgomery, and P. D. Reasor, 2002: A theory for the vertical alignment of a quasigeostrophic vortex. *J. Atmos. Sci.*, **59**, 150–168.

Schloemer, R. W., 1954: Analysis and synthesis of hurricane wind patterns over Lake Okechobee, FL. Hydromet report 31, Govt. Printing Office, No. C30,70:31.

Schneider, R. S. and G. M. Barnes, 2005: Low-level thermodynamic, kinematic, and reflectivity fields of Hurricane Bonnie (1998) at landfall. *Mon. Wea. Rev.*, **133**, 3243–3259.

Schubert, W. H., J. J. Hack, P. L. Silva, and S. R. Fulton, 1980: Geostrophic adjustment in an axisymmetric vortex. *J. Atmos. Sci.*, **37**, 1464–1484.

Schubert, W. H., M. T. Montgomery, R. K. Taft, T. A. Guinn, S. R. Fulton, P. Kossin, and J. P. Edwards, 1999: Polygonal eyewalls, asymmetric eye contraction, and potential vorticity mixing in hurricanes. *J. Atmos. Sci.*, **56**, 1197–1223.

Schubert, W. H., C. M. Rozoff, J. L. Vigh, B. D. McNoldy, and J. P. Kossin, 2007: On the

distribution of subsidence in the hurricane eye. *Quart. J. Roy. Meteor. Soc.*, **133**, 595–605.

Schwendike, J. and J. D. Kepert, 2008: The boundary–layer winds in Hurricanes Danielle (1998) and Isabel (2003). *Mon. Wea. Rev.*, **136**, 3168–3192.

Shapiro, L. J., 1983: The asymmetric boundary layer flow under a translating hurricane. *J. Atmos. Sci.*, **40**, 1984–1998.

———, 1992: Hurricane vortex motion and evolution in a three-layer model. *J. Atmos. Sci.*, **49**, 140–153.

Shapiro, L. J. and J. L. Franklin, 1995: Potential vorticity in Hurricane Gloria. *Mon. Wea. Rev.*, **123**, 1465–1475.

Shapiro, L. J. and J. Möller, 2003: Influence of atmospheric asymmetries on the intensification of Hurricane Opal: Piecewise PV inversion diagnosis of a GFDL model forecast. *Mon. Wea. Rev.*, **131**, 1637–1649.

———, 2005: Influence of atmospheric asymmetries on the intensification of GFDL model forecast hurricanes. *Mon. Wea. Rev.*, **133**, 2860–2875.

Shapiro, L. J. and H. E. Willoughby, 1982: The response of balanced hurricanes to local sources of heat and momentum. *J. Atmos. Sci.*, **39**, 378–394.

Shay, L. K., G. J. Goni, and P. G. Black, 2000: Effects of a warm oceanic feature on Hurricane Opal. *Mon. Wea. Rev.*, **128**, 1366–1383.

Simpson, R. H. and H. Riehl, 1958: Mid-troposphere ventilation as a constraint on hurricane development and maintenance. *Proc. Tenth Conf on Hurricanes, Miami Beach, FL*, AMS, D4.1–D4.10.

Smith, R. K., 1968: The surface boundary layer of a hurricane — Part I. *Tellus*, **20**, 473–483.

———, 1997: On the theory of CISK. *Quart. J. Roy. Meteor. Soc.*, **123**, 407–418.

———, 2000: The role of cumulus convection in hurricanes and its representation in hurricane models. *Rev. Geophys.*, **38**, 465–489.

———, 2003: A simple model of the hurricane boundary layer. *Quart. J. Roy. Meteor. Soc.*, **129**, 1007–1027.

Smith, R. K. and M. T. Montgomery, 2008: Balanced boundary layers used in hurricane models. *Quart. J. Roy. Meteor. Soc.*, **134**, 1385–1395.

Smith, R. K., M. T. Montgomery, and H. Zhu, 2005: Buoyancy in tropical cyclones and other rapidly rotating atmospheric vortices. *Dyn. Atmos. Oceans*, **40**, 189–208.

Smith, R. K., W. Ulrich, and G. Sneddon, 2000: The dynamics of hurricane-like vortices in vertical shear flows. *Quart. J. Roy. Meteor. Soc.*, **126**, 2653–2670.

Smith, R. K. and S. Vogl, 2008: A simple model of the hurricane boundary layer revisited. *Quart. J. Roy. Meteor. Soc.*, **134**, 337–351.

Terwey, W. D. and M. T. Montgomery, 2008: Secondary eyewall formation in two idealized, full-physics modeled hurricanes. *J. Geophys. Res.*, **113**, D12 112, doi:10.1029/2007JD008897.

Titley, D. W. and R. L. Elsberry, 2000: Large intensity changes in tropical cyclones: A case study of Supertyphoon Flo during TCM-90. *Mon. Wea. Rev.*, **128**, 3556–3573.

Tonkin, H., G. J. Holland, N. Holbrook, and A. Henderson-Sellers, 2000: An evaluation of thermodynamic estimates of climatological maximum potential tropical cyclone intensity. *Mon. Wea. Rev.*, **128**, 2000.

Tuleya, R. E., M. DeMaria, and J. R. Kuligowski, 2007: Evaluation of GFDL and simple statistical model rainfall forecasts for U.S. landfalling tropical storms. *Wea. Forecasting*, **22**, 56–70.

Velasco Fuentes, O. U., 2004: Vortex filamentation: its onset and its role on axisymmetrisation and merger. *Dyn. Atmos. Ocean.*, **40**, 23–42.

Vickery, P. J., P. F. Skerjl, A. C. Steckley, and L. A. Twisdale, 2000: Hurricane wind field model for use in hurricane simulations. *J. Engineering Structures*, **126**, 1203–1221.

Wakimoto, R. M. and P. G. Black, 1994: Damage survey of Hurricane Andrew and its relationship to the eyewall. *Bull. Amer. Meteor. Soc.*, **75**, 189–200.

Wang, Y., 2002a: Vortex Rossby waves in a numerically simulated tropical cyclone. Part I: Overall structure, potential vorticity, and kinetic energy budgets. *J. Atmos. Sci.*, **59**, 1213–1238.

———, 2002b: Vortex Rossby waves in a numerically simulated tropical cyclone. Part II: The role in tropical cyclone structure and intensity changes. *J. Atmos. Sci.*, **59**, 1239–1262.

———, 2008: Rapid filamentation zone in a numerically simulated tropical cyclone. *J. Atmos. Sci.*, **65**, 1158–1181.

Wang, Y. and G. Holland, 1996: Tropical cyclone motion and evolution in vertical shear. *J. Atmos. Sci.*, **53**, 3313–3332.

Wexler, H., 1947: Structure of hurricanes as determined by radar. *J. N. Y. Acad. Sci.*, **48**, 821–845.

Willoughby, H. E., 1978: A possible mechanism for the formation of hurricane rainbands. *J. Atmos. Sci.*, **35**, 838–848.

———, 1979: Forced secondary circulations in hurricanes. *J. Geophys. Res.*, **84C**, 3173–3183.

———, 1988: The dynamics of the tropical cyclone core. *Aust. Meteor. Mag.*, **36**, 183–191.

———, 1990a: Gradient balance in tropical cyclones. *J. Atmos. Sci.*, **47**, 265–274.

———, 1990b: Temporal changes of the primary circulation in tropical cyclones. *J. Atmos. Sci.*, **47**, 242–264.

———, 1991: Reply. *J. Atmos. Sci.*, **48**, 1209–1212.

———, 1995: Mature structure and evolution. *Global Perspectives On Tropical Cyclones*, Elsberry, R. L., Ed., World Meteorological Organisation, pp. 21–62.

Willoughby, H. E., J. A. Clos, and M. G. Shoreibah, 1982: Concentric eyewalls, secondary wind maxima, and the evolution of the hurricane vortex. *J. Atmos. Sci.*, **39**, 395–411.

Willoughby, H. E., R. W. R. Darling, and M. E. Rahn, 2006: Parametric presentation of the primary hurricane vortex. Part II: A new family of sectionally continous profiles. *Mon. Wea. Rev.*, **134**, 1102–1120.

Willoughby, H. E., F. D. Marks, Jr., and R. J. Feinberg, 1984: Stationary and moving convective bands in hurricanes. *J. Atmos. Sci.*, **41**, 3189–3211.

Willoughby, H. E. and M. E. Rahn, 2004: Parametric presentation of the primary hurricane vortex. Part I: Observations and evaluation of the Holland (1980) model. *Mon. Wea. Rev.*, **132**, 3033–3048.

Wong, M. L. M. and J. C. L. Chan, 2004: Tropical cyclone intensity in vertical winds shear. *J. Atmos. Sci.*, **61**, 1859–1876.

———, 2007: Modeling the effects of land-sea roughness contrast on tropical cyclone winds. *J. Atmos. Sci.*, **64**, 3249–3264.

Wroe, D. R. and G. M. Barnes, 2003: Inflow layer energetics of Hurricane Bonnie (1998) near landfall. *Mon. Wea. Rev.*, **131**, 1600–1612.

Wu, C.-C. and H.-J. Cheng, 1999: An observational study of environmental influences on the intensity changes of Typhoons Flo (1990) and Gene (1990). *Mon. Wea. Rev.*, **127**, 3003–3031.

Wurman, J. and J. Winslow, 1998: Intense sub-kilometre-scale boundary layer rolls observed in Hurricane Fran. *Science*, **280**, 555–557.

Yau, M. K., Y. Liu, D.-L. Zhang, and Y. Chen, 2004: A multiscale numerical study of Hurricane Andrew (1992). Part VI: Small-scale inner-core structures and wind streaks. *Mon. Wea. Rev.*, **132**, 1410–1433.

Zehr, R. M., 2003: Environmental vertical wind shear with Hurricane Bertha (1996). *Wea. Forecasting*, **18**, 345–356.

Zhang, D.-L., Y. Liu, and M. K. Yau, 2001: A multiscale numerical study of Hurricane Andrew (1992). Part IV: Unbalanced flows. *Mon. Wea. Rev.*, **129**, 92–107.